110

Modeling of Cone Deposition Process for Field Emitter Displays

by

James David De La Torre

Submitted to the Department of Electrical Engineering and Computer Science

in Partial Fulfillment of the Requirements for the Degrees of

Bachelor of Science in Electrical Science and Engineering

and Master of Engineering in Electrical Engineering and Computer Science

at the Massachusetts Institute of Technology

May 21, 1996

Author _____
Department of Electrical Engineering and Computer Science
May 21, 1996

Certified by _____
Tayo Akinwande
Thesis Supervisor

Accepted by _____
F. R. Morgenthaler
Chairman, Department Committee on Graduate Theses

Modeling of Cone Deposition Process for Field Emitter Displays

James David De La Torre

May 21, 1996

Abstract

The Field emitter display (FED) is a very promising type of flat panel display. It possesses the potential to combine the performance of the Cathode Ray Tube with the compactness of the Liquid Crystal Display, while offering the additional advantage of low power consumption. The performance and reliability of the FED depend strongly upon the geometry of the deposited emitter cones. The formation of this cone is affected by the geometry of the trench into which it is deposited, as well as processing parameters such as temperature and the angular distributiuon of deposition flux. The affect of each of these parameters upon evolution of the emitter cones is investigated, in an effort to eliminate much of the guesswork currently used when desigining processes to produce FED's. This study concludes that the parting layer angle and flux distribution are the most important factors influencing the final shape of the emitter cones.

Contents

1 Introduction and Overview

The field emitter display (FED) is a flat panel display technology which is currently under heavy research. It is potentially a replacement for the two predominant display types in use— the cathode ray tube (CRT) and the liquid crystal display (LCD). Before describing the FED, a brief overview of the CRT and LCD are in order.

1.1 Existing Display Technologies

1.1.1 The Cathode Ray Tube

The Cathode Ray Tube (CRT) is by far the most common type of display. It is the display technology which gives the best performance. The CRT operates using cathodoluminescence. Electrons are thermionically emitted from the gun and accellerated into the phosphors on the screen. The phosphors are excited by the electrons, and light is produced. In this way, the CRT has a built-in light source. This method of producing light is also very energy efficient, and different phosphor types allow the CRT to display all colors. The light produced is bright, exhibits good contrast, and can be viewed at any angle. CRT's offer high resolution, a fast refresh rate, and pixel addressability[1].

All these attributes make the CRT the display of choice. The problem with the CRT is not its performance, but rather its size. The deflection coils are large and heavy, and due to limitations of the beam deflecting hardware, as the size of a display increases, the depth of the CRT must also increase. Furthermore, this increase in volume requires that the glass of the CRT be made thicker, and thus heavier, to avoid implosion[1].

1.1.2 The Liquid Crystal Display

Portable display technology is growing in popularity, particularly in notebook computer displays. The requirements for such displays are that they consume as little power as possible, that they be small and lightweight, and that they deliver acceptable performance. All this must be accom-

plished at economically feasable prices, too.

The current display technology used in portable computers is Liquid Crystal Display, or LCD. LCD's operate by polarizing light. LCD's have a polarized backlight, which shines through a liquid crystal layer sandwiched between two panels of glass. Transparent conducting films are located on the inside surface of these panels. By applying voltages to the conducting films, an electric field is created, which acts to change the liquid crystals' orientation between the films. The oriented crystals act as a filter which can either pass or block the light from the backlight. On color displays, the front glass panel is covered with red, green, and blue dots (on the three color elements of each pixel) which act as filters, blocking other colors of light.

The performance of LCD's is not terrible, but a lot remains desired. Because the light emitted from LCD's is polarized, the viewing angle is very limited. The polarization complicates color LCD's, because the spectrum of each color filter must be matched with the spectrum of the light source[1]. This is what causes the color of LCD displays to appear different under different lighting conditions. A third disadvantage caused by the polarization is that LCD's cannot be viewed under bright light, since the incoming unpolarized light overwhelms the polarized light emitted from the display.

Liquid crystals does not exhibit a highly nonlinear polarization response to an applied voltage. This poses a disadvantage in that a large voltage swing is necessary to get a substantial range of polarization and thus pixel brightness. This also makes matrix addressing more complicated. Row/column matrix addressing schemes usually maintain unselected rows and columns at an equal neutral voltage. To select and address, the two lines (row and column) are set to voltages equal in magnitude but of opposite signs. Since the LCD response to the applied voltage is not very nonlinear, the difference in response between a selected address and an unselected address in the same row or column is not extremely large[1].

The capacitance associated with the liquid crystals limits the maximum refresh rate of LCD's. This creates the "shadowing effect" when objects on the display (such as a mouse pointer) move rapidly. The response time of the liquid crystals is also a function of temperature, and at low

temperatures, the response time becomes very slow. There are two types of LCD's– passive matrix LCD's (PMLCD's), and active matrix LCD's. In an AMLCD, a transistor is placed at each pixel to give a highly non-linear response. This increases the brightness range and speed of pixel response, but it does not eliminate the other problems of LCD's. Furthmore, AMLCD's are complicated and expensive to manufacture[1].

Perhaps the most important drawback of LCD's is the amount of power they consume. LCD's are fundamentally inefficient, because half of all the light is immediately filtered out by the back-light polarizer. Furthermore, the backlight is always on. The color filters also filter out most of the light that reaches them[1]. Thus, in order to achieve sufficient brightness in LCD's, much power is needed. The luminous efficieny of AMLCD's is approximately 1 lumen per watt. In notebook computers, display power consumption makes up about half of the total power consumed. Thus, the inefficiency of LCD's severely limits the battery life of notebook computers.

1.2 Field Emitter Displays (FED's)

The Field Emitter Display (FED) has the potential to combine the excellent performance of the CRT with the small size of the LCD, and it offers additional advantages over both display types.

The FED consists of an array of millions of tiny field emitters, like the ones shown in Figure 1. Each emitter is essentially a microscopic CRT, consisting of a metal cone, or tip, surrounded by a gate electrode. The anode is located on a glass front plate containing the phosphors. The emitters are located on a backplate (also made of glass) containing metallic electrode stripes. These stripes act as the row select lines, and the column select lines are formed by striping the gate layer in a similar fashion. The stripes are much larger than the individual emitters, giving about one thousand emitters per pixel. The structures are separated by about 200μm, using small glass spacers[2].

The emitters rely on electron tunnelling to emit electrons. When a large enough potential difference is applied between the gate and the emitter, electrons will tunnel out of the tip. Due to symmetry, the electrons due not collide with the gate, but instead are accellerated into the

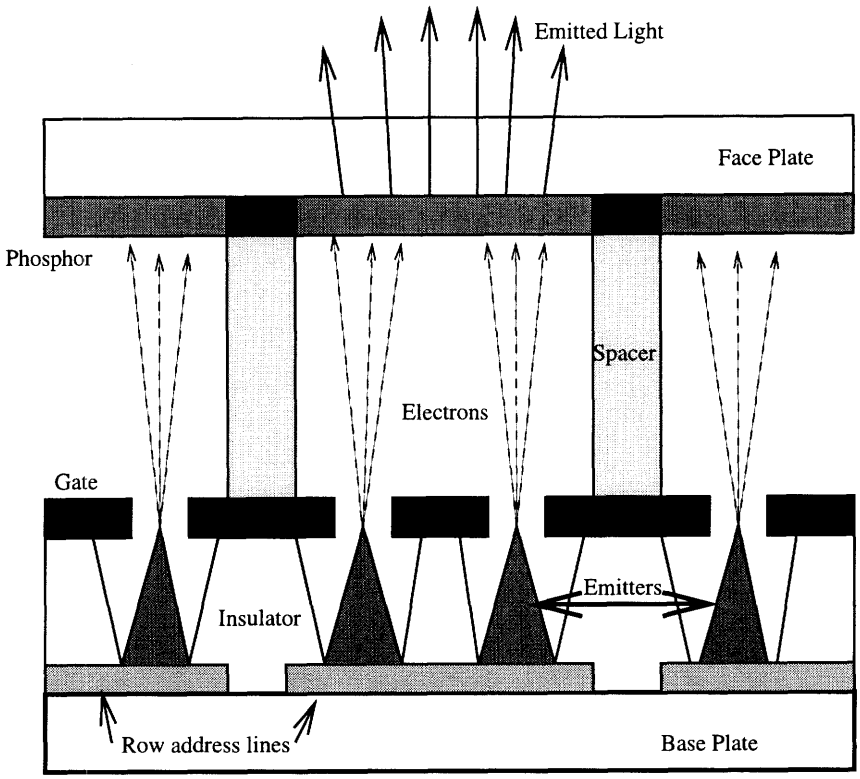

Figure 1: Individual Field Emitter

anode, which is biased positively with respect to the emitter and the anode. The electrons strike the phosphors, causing them to luminesce.

Thus, the operating principle of the FED is very similar to that of the CRT. However, the FED does not have the disadvantage of the CRT's large size. Field emitter arrays (FEA's) with tip to tip spacings as small as .32μm and as large as several microns have been produced. The gate to tip spacing has been varied from .08μm to about .5μm[3]. The thickness of the device, including the glass panels, is only about 2mm, and this thickness does not need to increase for larger area displays.

Clearly, the FED possesses the performance advantages of the CRT. It relies on cathodo-luminescence, giving a built-in light source, high brightness, excellent color, and wide viewing angle. The design allows for easy variation of voltages and currents, giving a wide range of pixel brightness. The individual emitters are very small, allowing for extremely high resolution. The tunnelling effect occurs very rapidly, so FED's can be refreshed at very high frequencies. The FED also has the advantage of small size, like the LCD, while maintaining excellent power efficiency.

The FED also possesses some of its own unique advantages. The nonlinearity of the tunnelling effect is extremely well-suited to matrix addressability, since a slight variation in gate to emitter voltage will produce a large change in the emission current. The individual emitters are much smaller than the size of the phosphors, so there are several hundred emitters per phosphor. The large number of emitters per pixel incorporates redundancy into the design, enabling pixels to work even when some emitters fail[4]. The redundancy also gives rise to an averaging effect across the emitters in a pixel. The large number of emitters per pixel implies that each pixel will have the same distribution of emitter sizes[2].

2 Importance of the Emitter Cone

Despite the many advatnages of the FED, it is not yet the dominant display technology. FED's are difficult to manufacture, and their reliability needs to be improved before they can become a real alternative to CRT's or LCD's. The critical element of a field emitter is the actual emitter cone. It is from the tip of the cone that the electrons are emitted.

2.1 Current Emission Properties

Electrons are emitted from the cones through electron tunnelling. The Fowler-Nordheim relation relates J, the field emission current density at a metal surface, to E, the electric field at that surface and ϕ, the material work function by the equation

$$J = \frac{AE^2}{\phi t^2(y)} exp(-B\frac{\phi^{\frac{3}{2}}}{E} v(y)), \tag{1}$$

where $A = 1.54 \times 10^{-6}$, $B = 6.87 \times 10^7$, and $y = \frac{3.79 \times 10^{-4} E^{\frac{1}{2}}}{\phi}$, the Schottky barrier lowering effect of the work function[4].

Spindt et al.[4], have shown that over the operating ranges of interest to FED's, that the functions $t(y)$ and $v(y)$ can be approximated as

$$t^2(y) = 1.1, \tag{2}$$

and

$$v(y) = .95 - y^2. \tag{3}$$

The electric field at the cone tip can be derived by modelling the tip of the cone and the gate as two concentric spheres[4], as shown in Figure 2. The inner sphere represents the tip of the emitter cone, where r is the radius of curvature at the tip. The outer sphere represents the gate aperture, with radius R.

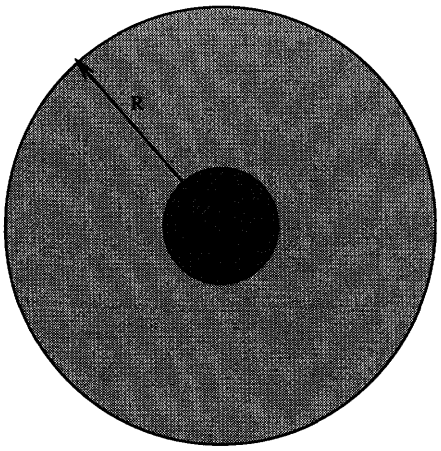

Figure 2: Diagram of two concentric spheres. The small sphere represents the tip of the emitter with radius of curvature r. The large sphere respresents the gate aperture radius, R.

The equation describing the electric field at the tip is thus

$$E_{tip}(r) = \frac{V}{r}\frac{(R+r)}{R} = V(\frac{1}{r} + \frac{1}{R}). \tag{4}$$

Substituting into the relation $E_{tip} = \beta V$, where β is the field enhancement factor at the tip, gives

$$\beta = (\frac{1}{r} + \frac{1}{R}). \tag{5}$$

The emitter current, I, is simply $\frac{J}{\alpha}$, where α is the area of the emitting surface and is proportional to r^2.

Substituting these relationships into Equation 1, yields

$$I = aV^2 exp(\frac{-b}{V}), \tag{6}$$

where

$$a = \frac{\alpha A(\frac{1}{r} + \frac{1}{R})^2}{1.1\phi} exp(\frac{B(1.44 \times 10^{-7})}{\phi^{\frac{1}{2}}}), \tag{7}$$

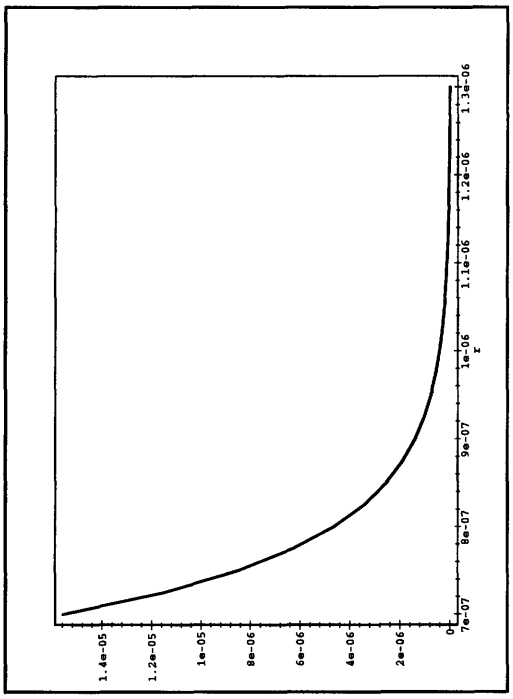

Figure 3: Current emitted at 50V for R=.5μm and uniform distribution of r.

and

$$b = \frac{0.95B\phi^{\frac{3}{2}}}{(\frac{1}{r} + \frac{1}{R})} \tag{8}$$

Thus, for a given R, α, and ϕ, the current at a fixed voltage, V, can be determined as a function of r, the radius of tip curvature. Figure 3 gives a plot of the tip emission current as a function of r at $V = 50V$ for an emitter with $R = .5\mu$m, $\alpha = r^2$, and $\phi = 4.5$eV. In the figure, r is varied from 7nm to 13nm. Notice how as r decreases, the emission current rises dramatically. Figure 3 assumes that there is a uniform distribution of tip radii of curvature. Figure 4, on the other hand, assumes that the tip sizes follow a Gaussian distribution, with mean radius $\bar{r}$=100$\mathring{A}$ and standard deviation of 10$\mathring{A}$. In this figure, the maximum current density results at $r = 88\mathring{A}$.

The two figures imply that very small variations in the radius of curvature of the cone tips will yield large variations in emitter current. If the radius of curvature is too large, the tip may not emit enough current, while if it is too small, the tip may burn out easily and exhibit poor reliability[4].

The geometry of the emitter cone also affects the capacitance between the tip and substrate.

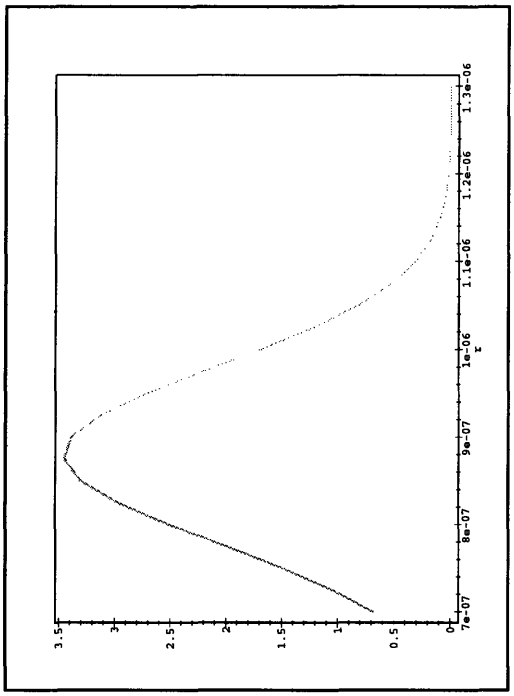

Figure 4: Current emitted at 50V, for R=.5μm, assuming Gaussian Distribution $\bar{r} = 100\mathring{A}$, $\sigma_r = 10\mathring{A}$.

The optimum shape for an emitter was shown to be a "rounded whisker"— a tall and thin vertical pillar with a hemispherical top[6]. To emulate this as closely as possible, a long, narrow cone is desirable. This shape will yield a low capacitance and therefore low leakage current, low dynamic power dissipation, and fast switching speed[3]. It is therefore desirable to be able to manufacture cones that are very sharp (small tip radius of curvature), and that are very tall and narrow.

Thus, in order for FED's to perform well, the emitter cones must be able to be fabricated correctly, predictably, and uniformly. This makes the fabrication process of the cones very critical to device performance.

2.2 Cone Fabrication and Important Process Parameters

2.2.1 Deposition Process

In order to produce cones of desired geometries, their deposition process must be understood. Figures 5-7 show the trench/cone fabrication process. The cones are deposited by electron-beam deposition into the cylindrical trenches. The trenches are composed of silicon dioxide sidewalls

with a molybdenum bottom. The molybdenum gate layer is on the top of the structure.

Before the cones are deposited, a parting layer of aluminum is deposited onto the gate layer. This is done for the liftoff step, which occurs after the cone deposition. The parting layer is deposited by electron beam deposition at a grazing angle to the wafer surface normal[4].

Once the parting layer is deposited, the actual molybdenum cone deposition is carried out, also by electron beam deposition. During the deposition process, impinging molybdenum atoms adhere to the parting layer, and over time, the trench opening narrows and eventually closes. Thus, the region inside the trench where unobstructed flux may land also narrows with time. It is this phenomenon which gives the deposited emitters their conic shape. In addition to the vertical flux of atoms, however, a lateral flux will occur, due to surface self diffusion. The final shape of the cones will not be perfect geometric cones, but will be slightly different, depending upon the relative rates of vertical flux, trench closure, and surface diffusion[7]. The geometry of the trench (parting layer shape, and initial trench opening radius), as well as various process parameters (temperature, degree of flux collimation) and material parameters (diffusion coefficient, surface tension) affect the evolution of the cones with time.

Many parameters influence the resulting shape of deposited emitter cones. The deposition temperature and material parameters, the parting layer angle and thickness, and the angular distribution of incoming flux all affect the cone evolution in some way. Each of these parameters are discussed below.

2.2.2 Temperature and Surface Diffusion

Temperature is important to the cone deposition process because it affects the amount of surface diffusion that will occur. Surface diffusion results when atoms impinging upon a surface migrate in such a manner as to decrease their chemical potential[7,8,9]. There exists a relationship between the curvature and the chemical potential of a point on a surface. It can be shown that the increase in the chemical potential of an atom moving from a point of zero curvature to a point of curvature K is

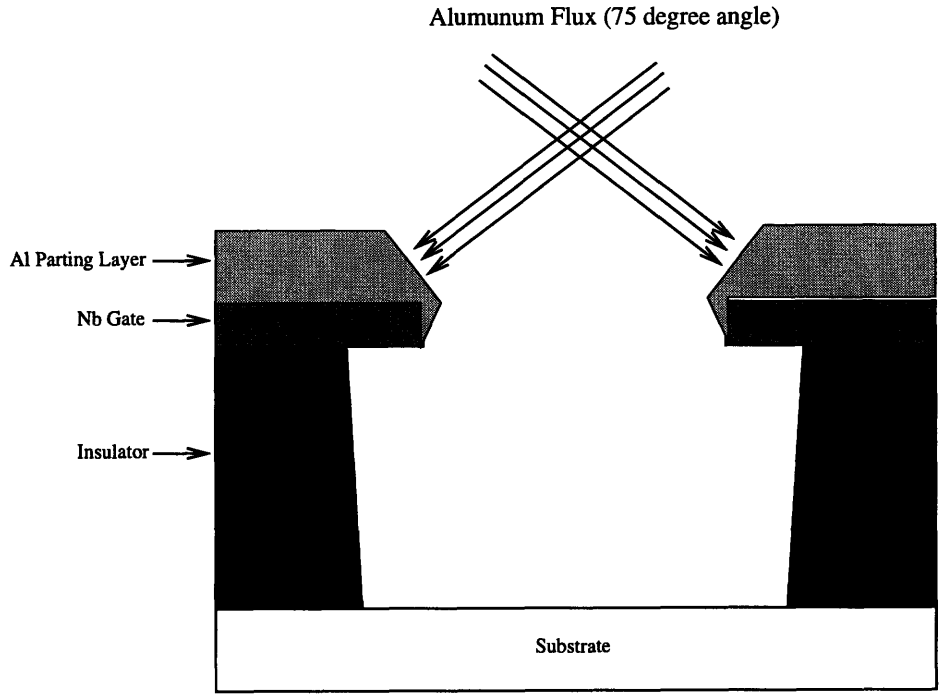

Figure 5: Angled deposition of Parting Layer onto substrate.

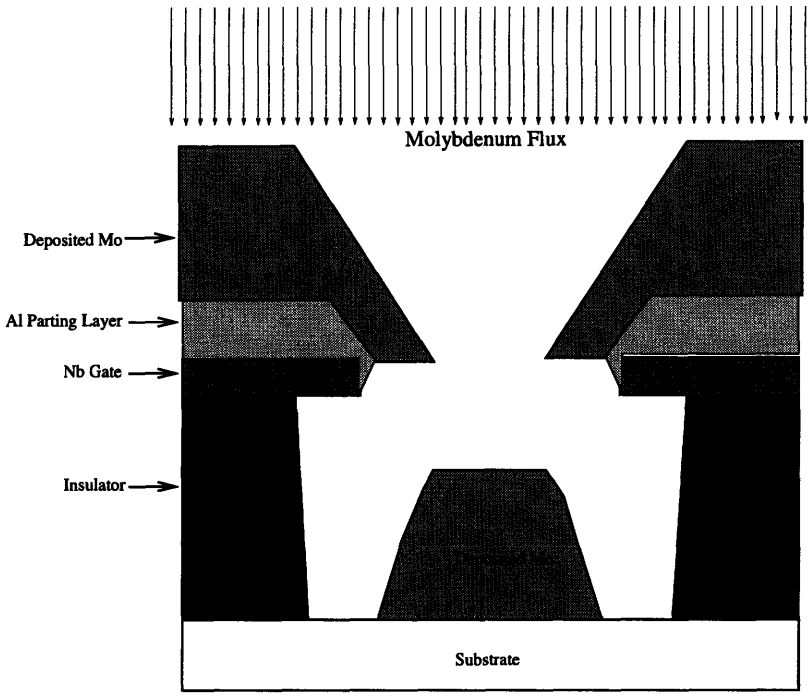

Figure 6: Molybdenum cone halfway through the deposition process.

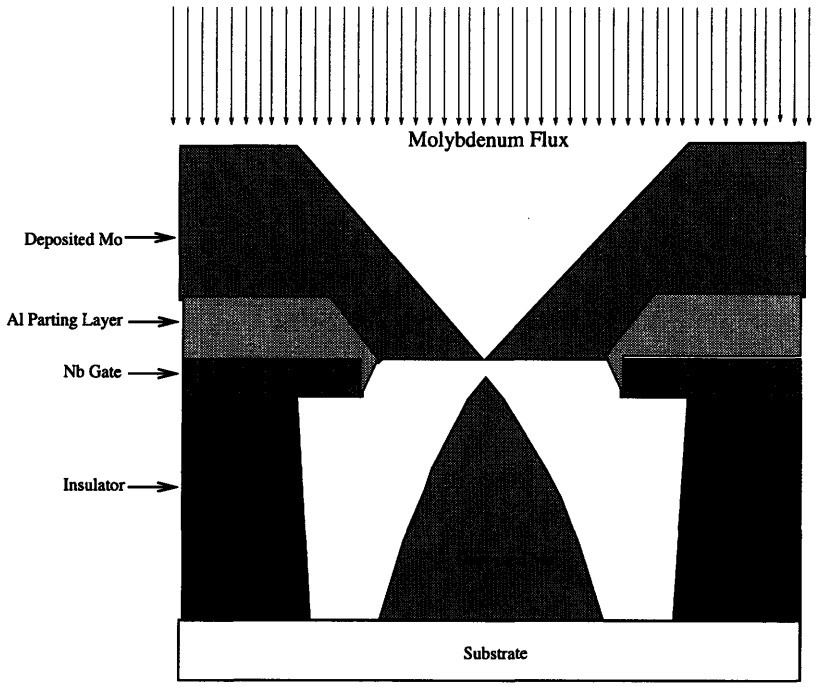

Figure 7: Molybdenum cone at completion of deposition process.

$$\mu(K) = K\gamma\Omega, \tag{9}$$

where γ is the surface tension (in $\frac{eV}{cm^2}$), and Ω is the atomic volume (cm^3).

Thus, on a surface with gradients in curvature, there will exist a corresponding gradient in chemical potential. The gradient in chemical potential will cause atoms to drift along the surface with a velocity, V, given by

$$V = -\frac{D_s}{kT}\frac{\delta\mu}{\delta s} = -\frac{D_s\gamma\Omega}{kT}\frac{\delta K}{\delta s}. \tag{10}$$

D_s is the surface diffusivity ($\frac{cm^2}{s}$), which is thermally activated and can be expressed as

$$D_s = D_0 exp(\frac{-E_A}{kT}), \tag{11}$$

and s is the arc length along the surface[9].

For a given density of surface atoms, ν (cm^{-2}), the flux of atoms is simply

$$J = -\nu \frac{D_s \gamma \Omega}{kT} \frac{\delta K}{\delta s}. \tag{12}$$

By taking the surface divergence of -J, the increase of atoms per unit area per unit time is obtained. For a one-dimensional case, the derivative along the surface is used. To calculate the rate of growth normal to the surface, r_n, simply multiply by Ω[9]. The resulting equation is thus

$$r_n = \frac{D_s \gamma \Omega^2 \nu}{kT} \frac{\delta^2 K}{\delta s^2}. \tag{13}$$

This rate can be expressed as a projection of the vertical growth of a surface ($\frac{\delta z}{\delta t}$) onto the surface normal, yielding the relation

$$r_n = (1 + (\frac{\delta z}{\delta x})^2)^{-\frac{1}{2}} (\frac{\delta z}{\delta t}). \tag{14}$$

An equation in the form of $z(x,t)$ can be obtained by substituting this equation and the definition of curvature,

$$K = -\frac{\frac{\delta^2 z}{\delta x^2}}{(1 + (\frac{\delta z}{\delta x})^2)^{\frac{3}{2}}} \tag{15}$$

into Equation 13, and by using the relation $\frac{\delta}{\delta s} = (\frac{\delta x}{\delta s}) \times (\frac{\delta}{\delta x})$. The resulting equation, which relates the vertical growth rate of a surface due to surface diffusion, is thus

$$\frac{\delta z}{\delta t} = -\frac{D_s \gamma \Omega^2 \nu}{kT} \frac{\delta}{\delta x} [(1 + (\frac{\delta z}{\delta x})^2)^{-\frac{1}{2}} \frac{\delta}{\delta x} (\frac{\frac{\delta^2 z}{\delta x^2}}{(1 + (\frac{\delta z}{\delta x})^2)^{\frac{3}{2}}})] \tag{16}$$

Mullins has studied surface diffusion phenomena where the slope ($\frac{\delta z}{\delta x}$) of the structures under observation was much less than unity[9]. This allowed him to simplify Equation 16 into $\frac{\delta z}{\delta t} = -\frac{D_s \gamma \Omega^2 \nu}{kT} \frac{\delta^4 z}{\delta x^4}$. This assumption is not valid when studying emitter cones, because their sides have slopes much greater than unity. Indeed, the larger the slope of cone's sides, the more desirable it is, since a tall and narrow cone has a small capacitance. Therefore, the general equation must

be used when modelling surface diffusion of the emitter cone structures. Defining the surface diffusion coefficient, $B = \frac{D_s \gamma \Omega^2 \nu}{kT}$, and expanding Equation 16 into distinct terms yields

$$\frac{\delta z}{\delta t} = -B\lambda^{-2}\frac{\delta^4 z}{\delta x^4} - 10\lambda^{-3}\frac{\delta z}{\delta x}\frac{\delta^2 z}{\delta x^2}\frac{\delta^3 z}{\delta x^3} - 3\lambda^{-3}(\frac{\delta^2 z}{\delta x^2})^3 + 18\lambda^{-4}(\frac{\delta z}{\delta x})^2(\frac{\delta^2 z}{\delta x^2})^3, \tag{17}$$

where $\lambda = 1 + (\frac{\delta z}{\delta x})^2$. This is a fourth-order, nonlinear, non-variable-separable equation.

The amount of surface diffusion that will occur during deposition is strongly dependent upon temperature, the preexponential coefficient, D_0, and the activation energy, E_A, of the material being deposited. Most diffusion data that exists for molybdenum has been collected in experiments at temperatures between 1200-2700K[8,11]. This is much higher than is used in the deposition of the emitter cones (room temperature, 300K). Furthermore, the values determined for D_0 and E_A in these experiments vary by as much as four orders of magnitude and 100%, respectively[8]. The same is true for other metals used for field emitter arrays[8]. Aluminum, on the other hand, has been studied at room temperature[10], and the experimentally determined values correlate well with the observed behavior.

Cale, et al.found the values for aluminum to be $D_0 = 6 \times 10^{-4} \frac{cm^2}{s}$, and E_A=.5eV[10]. As previously noted, several values for molybdenum have been published. For the purposes of this thesis, the values of D_0=370$\frac{cm^2}{s}$ and E_A=3.26eV were used. These values were determined by grain boundary grooving methods, at temperatures between 1820K and 2620K[8]. This set of values was chosen because they were derived by grain boundary grooving, and they were derived at the lowest temperatures of all the available data.

Another material parameter which determines the value of surface diffusion is γ, the surface tension. Tyson, et. al. have published surface tension data for many metals, including aluminum and molybdenum. The values used were γ_{Al}=6.88$\times$10^{14} $\frac{eV}{cm^2}$ and γ_{Mo}=1.81$\times$10$^{15}\frac{eV}{cm^2}$, respectively[12].

Substituting the appropriate values in for B gives at 300K,

$$B_{Al} = 1.06 \times 10^{-18}, \tag{18}$$

and

$$B_{Mo} = 6.87^{-59}. \tag{19}$$

Thus, the diffusion coefficient for Mo based on the published data is virtually zero at room temperature, and is forty orders of magnitude smaller than B_{Al}. Preliminary experiments carried out using the process simulator SPEEDIE (discussed below) showed that there was no evidence of any molybdenum surface diffusion occurring at temperatures up through 500K. Aluminum, however, exhibited a definite activation at temperatures very close to 300K. Because of this, it was decided that the diffusion data for aluminum would be used in the experiments. In this way, the importance of surface diffusion could be compared to other parameters of the cone deposition process.

2.2.3 Parting Layer Bevel and Thickness

During the fabrication process of field emitters, the trench opening is formed by etching the gate layer. This is done either by reactive ion etching or chemical etching. Depending upon the manner in which the gate layer is etched, its inner surface (the surface which defines the radius of the trench), will have a bevel to it[7]. Figure 8 shows some example bevels of the gate layer.

After the gate layer and underlying oxide has been etched, the parting layer is deposited at grazing incidence. The parting layer will also have a bevelled surface which depends upon its deposition angle and the gate layer bevel.

The parting layer bevel affects the evolution of the cones because the Molybdenum layer grows on the parting layer with a degree of conformality. Thus, a bevelled parting layer will cause the Molybdenum layer to grow along the surface normal of the parting layer, causing the trench opening to shrink and eventually close. The hypothesis was that tallest cones would result when the parting layer bevel was closest to vertical, because a near-vertical parting layer presents very little surface for the flux to build upon.

The thickness of the parting layer may also affect the shape of the emitter cones. A larger bevelled surface may cause the profile of the depositied metal to more closely track the bevel than

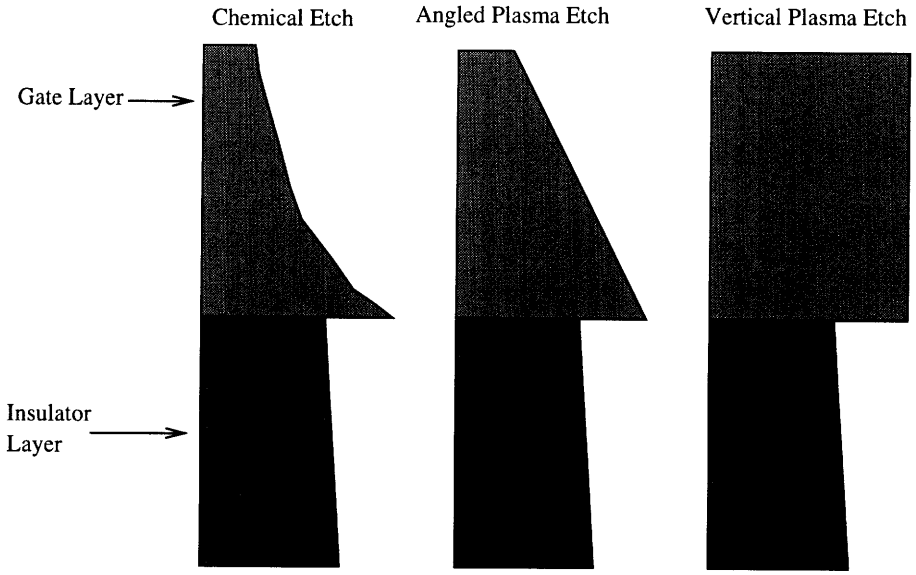

Figure 8: Gate bevels resulting from various etch methods.

the flat regions surrounding it. For completeness, it is investigated in the experiments.

2.2.4 Flux Distribution

The directionality of the flux plays an important role in the shape of the deposited cones. It is a parameter controlled by the processing equipment being used. A highly directed flux implies that the incoming molybdenum comes down at nearly perfectly normal incidence. Very little flux arrives from an angle. A widely distributed flux will cause Molybdenum to hit the substrate at off-normal angles. This has two effects upon the shape of the cone. The first is that regions that would normally be obstructed by the closing trench will receive incoming flux. This acts to increase the width of the cones. The second effect is that the off-vertical flux will act to close the trench more quickly. Since the parting layer is bevelled, the off-vertical flux actually arrives at the parting layer surface at an angle closer to normal incidence. This builds up the surface more rapidly, increasing the rate of trench closure. This will result in shorter cones. Thus, the relationship between flux distribution and cone height is a complex one. It was initially hypothesized that for

a widely distributed flux, the resulting cone heights would be lower than for a perfectly collimated flux.

2.3 Thesis Objectives

Currently, the relative importance of each parameter in the cone deposition process is not well understood. To produce cones of desired geometries, guesswork, empirical data, and trial and error methods are used. If the effects of each of the system parameters were understood, then these parameters could be set appropriately during the fabrication process to produce cones with the desired shapes. A better understanding of these parameters would help to decrease the cost of new process development, and existing processes could be optimized more effectively.

3 Computer Simulation Experiments

Two different approaches were used to model the cone deposition process. The first used a computer program written by the author, and the second utilized SPEEDIE, a process simulation tool from Stanford University.

3.1 Numerical Computer Simulation

The numerical simulation program modelled the evolving emitter cone. The program assumed an initial trench opening radius that closed linearly with time. The cone was formed by flux landing in the open area of the trench and diffusing away due to curvature gradients. The diffusion term was calculated directly from Equation 16. The simulation assumed a quasistatic situation in which the surface diffusion occurred much more rapidly than the deposition. The arriving flux at a given instant in time was allowed to redistribute and incorporate itself into the surface before new flux arrived in the next instant.

The program functionality is depicted schematically in Figure 9. First, all the exposed region of the trench receives an incremental unit of vertical flux. The exposed region is initially the radius of the trench, but it shrinks at a constant rate. After the deposition of the vertical flux, the first four derivatives at every point along the profile (both exposed and unexposed) are calculated. These values are then substituted into Equation 17. Finally, all points along the profile are modified due to the calculated surface diffusion height change. This process is repeated until the simulation time has expired. The program allows for diffusion to occur even at points where no flux is landing. This is an interesting feature of the program, because it allows for the examination of annealling effects on the cone structure.

Due to problems with numerical instability, it was difficult to get the program to work properly. The error associated with the higher-order derivatives compounded with the multiplication of the derivatives with each other made the program very sensitive to changes in material parameter values and timestep and spatial-step sizes. Thus, the parameter inputs to the program were not

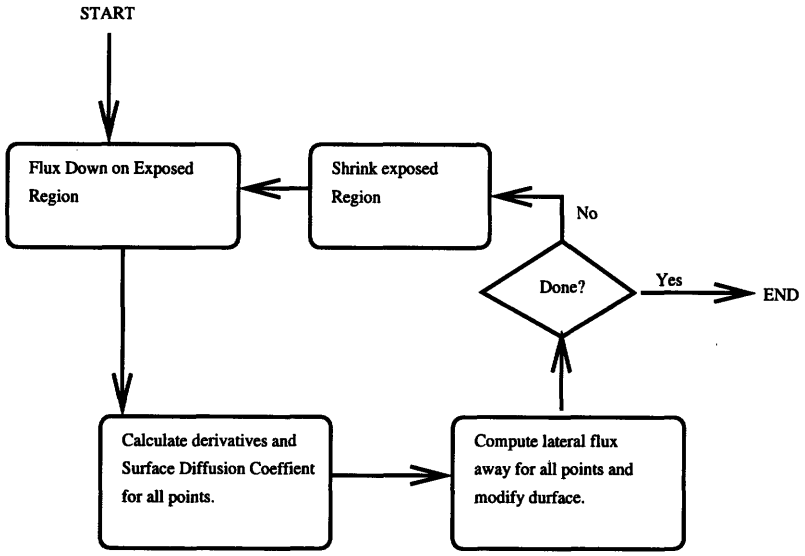

Figure 9: Flowchart of numerical deposition simulation program operation.

physically realistic. The surface diffusion coefficient of the material being deposited had to be made very large in order to see the effects of surface diffusion. Despite this fact, the output of the program provided a qualitative understanding of the effects of surface diffusion on the evolution of the cones with time.

The program results showed that over time, the cones smooth out, into a shape that almost resembles a Guassian. Annealling the cones also causes the radius of curvature at the tips to increase. This is an indication that surface diffusion is detrimental to the the performance of FED's, since a small radius of tip curvature is desired. Figure 10 shows a cone deposited with no surface diffusion, a cone deposited with surface diffusion, and a cone with diffusion that has been annealled.

3.2 Preliminary SPEEDIE Simulations

The majority of the results obtained in this thesis were through the use of the process simulation tool SPEEDIE (Stanford Etch and Deposition Profile Simulator). This tool allows the simulation of physical vapor deposition (PVD) processes, and it has the ability to incorporate surface diffusion

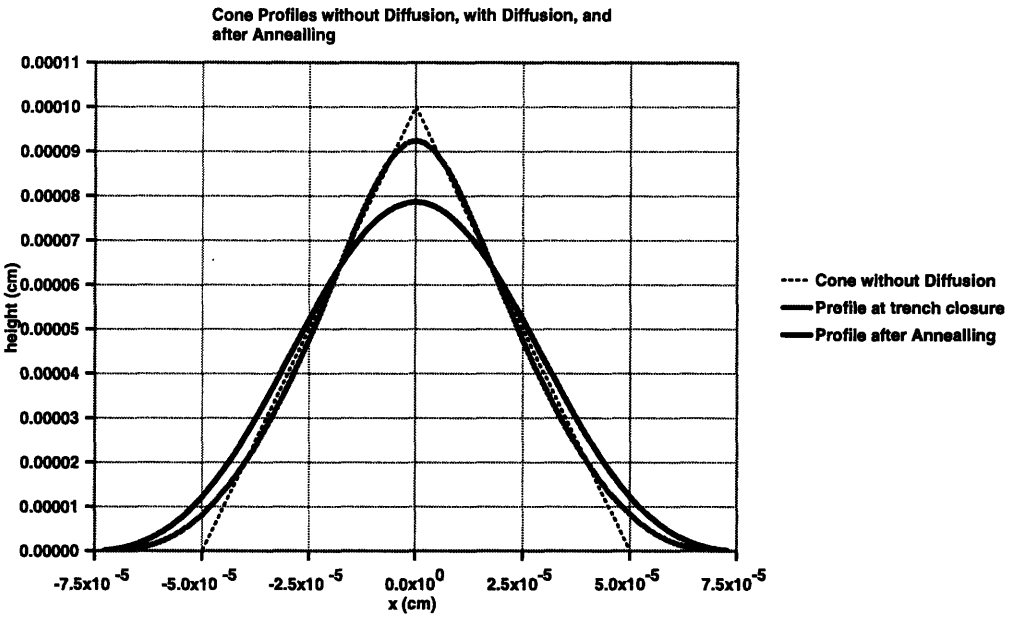

Figure 10: Graph showing Cones resulting with and without surface diffusion, and profile after annealling.

into its calculations of profile evolution. It takes as input the process parameters of simulation time, temperature, rate of flux, and uses material parameters density, surface tension, sticking coefficient, surface diffusivity, D_0, and the surface diffusion activation energy, E_A.

To gain an understanding of the important parameters in the deposition process, several preliminary simulations were run, using various starting substrates.

All substrates had a gate opening radius of .5μm, and were 1μm deep from the bottom of the trench to the bottom of the gate layer. The deposition rate of Molybdenum was set to 1μm per hour for all experiments.

3.2.1 Deposition on Simple Substrate

The first set of simulations run used the substrate in Figure 11. This substrate was composed of a .3μm thick gate layer with vertical sidewalls on top of the SiO_2 trench. In this set of simulations, the aluminum parting layer was deposited onto the substrate at a 75 degree angle. The deposition was carried out at room temperature for 15 minutes at 1μm per hour, giving a parting layer

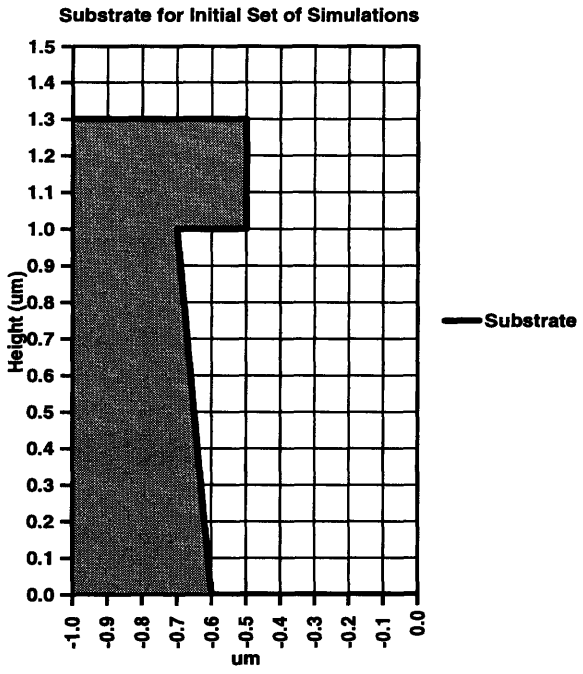

Figure 11: Substrate used in initial SPEEDIE simulations.

thickness of .25μm. For this substrate, the temperature of the aluminum deposition did not affect the resulting parting layer profile.

Once the parting layer was deposited, the molybdenum deposition was carried out. Several molybdenum deposition simulations were run at different temperatures and flux distributions. The temperatures used ranged from 2K to 500K. Because the diffusion coefficient of molybdenum taken from the literature[8] was so low in comparison to that of Aluminum[10], the aluminum values for D_0 and E_A were used in place of the values for molybdenum. Simulations showed that when using the diffusion data for molybdenum, no measurable surface diffusion occurred, even for temperatures above 500K. On the other hand, the values in the literature for aluminum give a diffusion coefficient that shows an sharp activation near 300K. The wide range in temperature used in the simulations allowed for the examination of depositions in which surface diffusion was essentially nonexistent, and when it was highly-activated.

The flux distributions used were either a perfectly collimated flux, where points on the surface

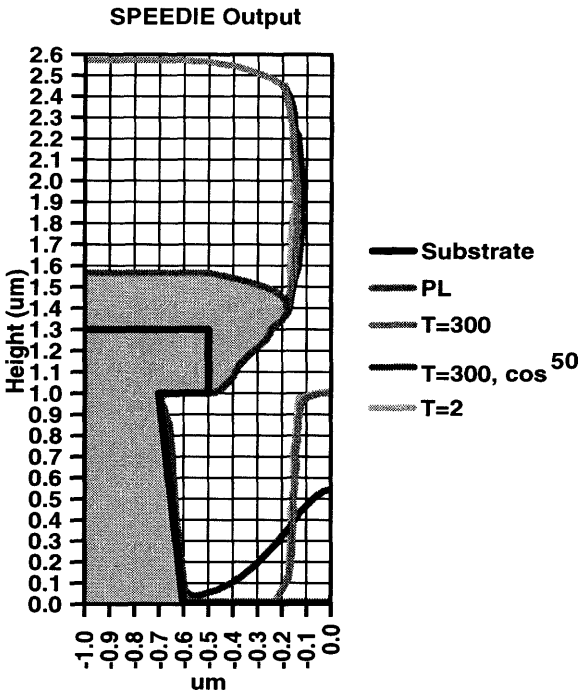

Figure 12: Results of Deposition on unbevelled substrate. No trench closure occurred.

only receive flux at normal incidence, or a $\cos^n(\theta)$ distributed flux. In the latter case, points on the surface receive a quantity of flux from an angle θ off-vertical which is proportional to $\cos^n(\theta)$. Thus, the larger the exponent n is, the more collimated the flux.

Figure 12 shows some results obtained from these simulations. Contrary to what was expected, the trench did not close for any of the simulations. Slight closure did occur for widely distributed fluxes, but for these cases the molybdenum in the trench formed more of a "lump" than a cone. The radius of the cones at the base of the trench were larger for distributed fluxes than for the collimated flux. In the simulations using tightly distributed fluxes, the molybdenum grew vertically in the trench and did not narrow appreciably with height.

3.2.2 Deposition on Bevelled Substrate

Since it is known that in reality the trench does actually close, another set of simulations was run in an effort to achieve trench closure. It was hypothesized that the parting layer in the first

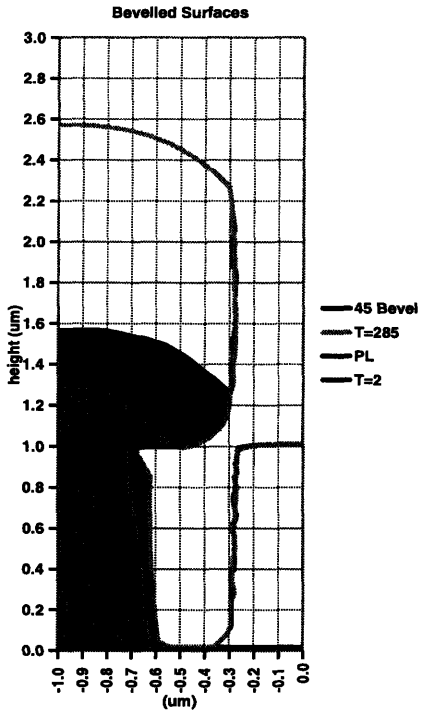

Figure 13: Results of Deposition on Substrate with 45 degree gate layer bevel. No Trench closure occurs

set of experiments did not have a bevel sharp enough to cause trench closure. It was proposed that by bevelling the gate layer of the substrate, the parting layer profile would conform to that surface and result in a more pronounced bevel. The bevelled substrate also represents a physcially realistic situation, in that the gate layer may possess a bevel depending upon the manner in which the opening is etched.

Thus the second set of simulations were carried out, using the bevelled substrate as the initial structure. The bevel was defined as the angle off-horizontal made by the gate layer. Bevels of 45 and 60 degrees were used in the simulations. Temperature was also varied, and the collimated flux distribution was used.

The results of these simulations showed that the parting layer did indeed exhibit more pronounced bevel than with the unbevelled substrate. However, the deposited molybdenum still did not cause the trench to close. Figures 13 and 14 show some of the results of these simulations.

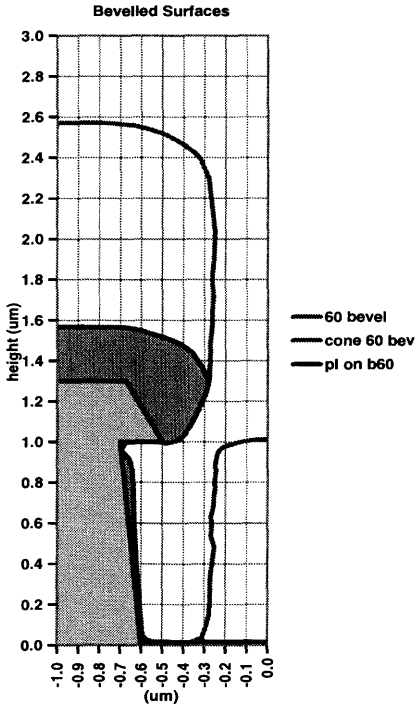

Figure 14: Results of Deposition on Substrate with 60 degree gate layer bevel. No trench closure occurs

3.2.3 Deposition on Substrate with Preexisting Bevelled Parting Layer

A hypothesis was made that the reason the trench was not closing in the first two sets of simulations was because of the rounded shape of the parting layer. To test this hypothesis, a third set of simulations were carried out using a substrate with a preexisting parting layer. This parting layer was .5μm thick and was given a bevel and a sharp edge at the trench opening. In this set of experiments, only the bevel and the deposition temperature were varied. Parting layer bevels of 45, 60, and 75 degrees were used in these simulations.

This set of simulations yielded interesting results, some of which are graphed in Figures 15-17. At low temperatures, substantial trench closure occurred in all cases, while at high temperatures, the trench did not close at all. It was observed that at low temperatures, material which landed on the bevelled parting layer did not move; it built up and closed the trench. In the high temperature regime, on the other hand, the flux which landed on the parting layer diffused completely and simply grew vertically with no trench closure. The temperature range over which this change occurred was extremely small. Figure 15 shows the resulting cone profiles for depositions which occurred at 305 and 306K on the substrate with the 45 degree parting layer bevel. Simulations conducted at intermediate temperatures, where some surface diffusion occurred but the trench still closed, showed that the trench closed the fastest for the 45 degree bevel and slowest for the 75 degree bevel. The same trend was observed for the low temperature simulations, which can be seen in Figures 15-17.

One additional simulation was run at 300K, using the collimated distribution and a substrate with a 45 degree bevel. The substrate differed from the one used in the previous set of simulations, in that the parting layer thickness was made to be only .2μm. This simulation was carried out to determine whether or not the thickness of the parting layer affected the trench closure rate. The result, plotted in Figure 18, indicated that the trench closed more quickly for the substrate with the thin parting layer.

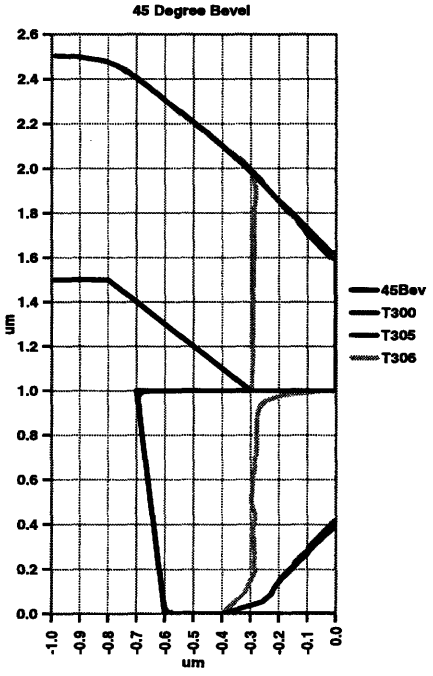

Figure 15: Results of Deposition onto substrate with 45 degree parting layer bevel. Not that the temperature transition between no surface diffusion and complete diffusion is less than 1 degree wide.

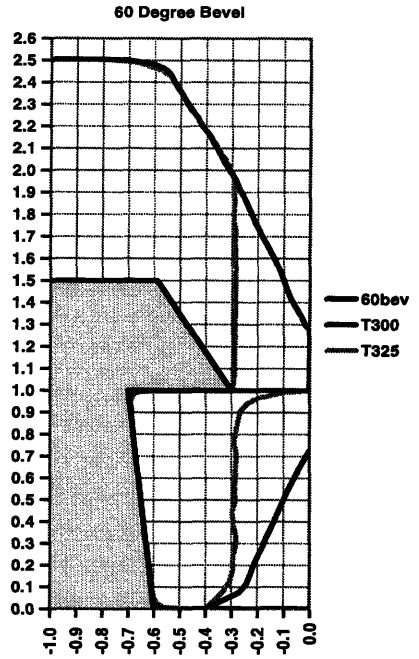

Figure 16: Results of Deposition onto substrate with 60 degree parting layer bevel.

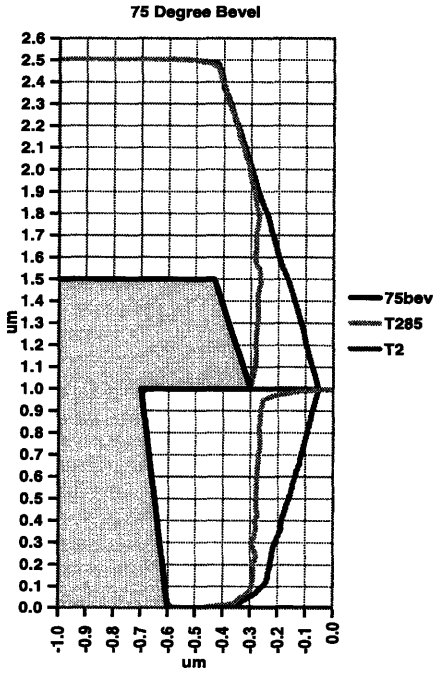

Figure 17: Results of Deposition onto substrate with 75 degree parting layer bevel.

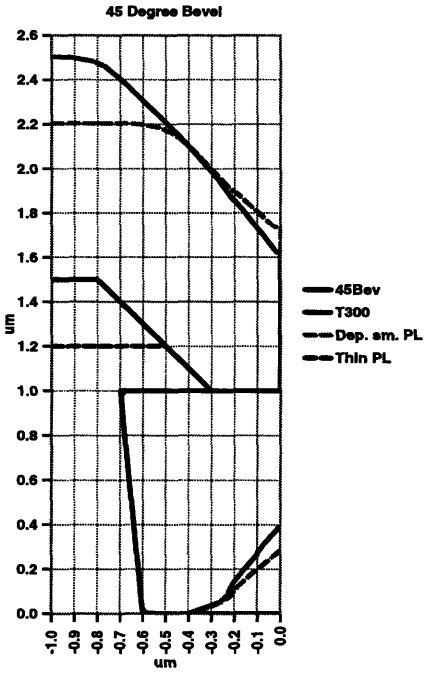

Figure 18: Results of deposition onto substrate with 45 degree parting layer bevel for both normal and thin parting layers. Note that the trench closes more quickly for the thin parting layer.

3.2.4 Findings of the Preliminary Simulations

The preliminary simulations yielded information upon which further simulation experiments were based. They demonstrated that the degree of flux collimation affects the shape of the cone and the trench closure rate. They showed that in order to achieve trench closure, an acute angle is needed at the edge of the parting layer where it overhangs the trench. They showed that at the temperatures of interest, molybdenum exhibits negligible surface diffusion, and that for the diffusion parameters being used (those of aluminum), the transition between no surface diffusion and highly activated surface diffusion is very sharp, and it occurs close to 300K. The simulations showed that the parting layer bevel is very important in determining trench closure rate, and that the thickness of the parting layer affects the closure rate as well.

3.3 Four-Parameter Binomial Simulation Experiment

With these results in mind, a binomial set of simulations was conducted in which the variables of temperature, flux distribution, parting layer bevel, and parting layer thickness were used.

3.3.1 Parameters Used

Temperature was set to either 2K or 310K. These two temperatures were chosen to obtain the effect of low and high diffusion coefficients.

Two flux distributions were used— a perfectly collimated distribution and a $\cos^{100}(\theta)$ distribution. In the latter distribution, the arriving flux falls to 50% of its maximum value by 7 degrees off-vertical, and it falls to 10% by 12 degrees.

Parting layer bevels of 30 degrees and 75 degrees were used. This allowed for the examination of very shallow and very sharp parting layer bevels.

The thickness of the parting layer was set to either .2μm or .4μm. These values are realistic values that may be used in the actual fabrication of the cones.

The substrate used in this set of simulations was slightly different than the ones used in other simulation sets. It had a bevelled parting layer (which was either .2μm or .4μm thick) on top of

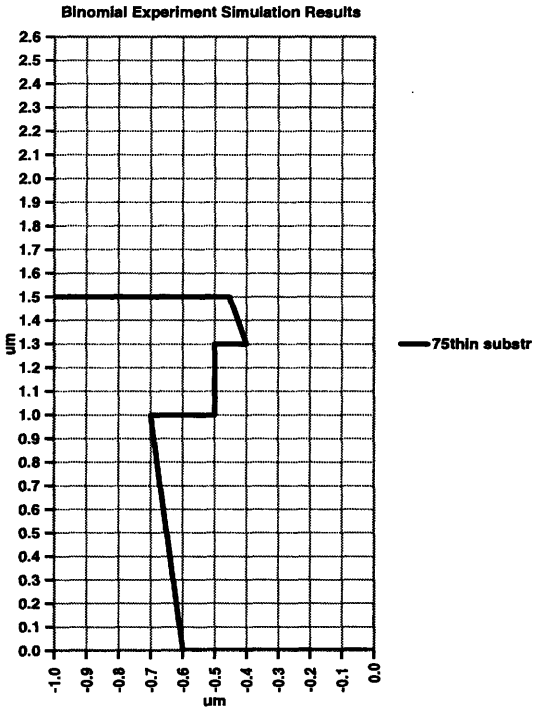

Figure 19: Example substrate used in binomial simulation set. Other substrates had .4μm thick parting layers and/or 30 degree bevels.

and slightly overhanging a gate layer with vertical sidewalls, which was .3μm thick. Figure 19 shows the substrate with the 75 degree bevel and .2μm thick parting layer.

With four parameters, each having two possible values, sixteen simulations were carried out to sample all possible parameter value combinations. All the resulting profiles are plotted in Figures 20-23.

3.3.2 Quantities Observed

From the results of each simulation, three values were calculated— the trench closure rate (TCR, $\frac{\mu m}{hr}$), the final cone height (FCH, μm), and the cone growth rate (CGR $\frac{\mu m}{hr}$).

The TCR for simulations in which the trenches did not close was simply equal to the distance that the trench closed during the simulation. For simulations in which the trenches did close, the thickness of the molybdenum layer deposited *on the parting layer* at the center of the trench, T_{Moc}, was measured (see Figure 24). Since the total simulation time was 1 hour and the molybdenum

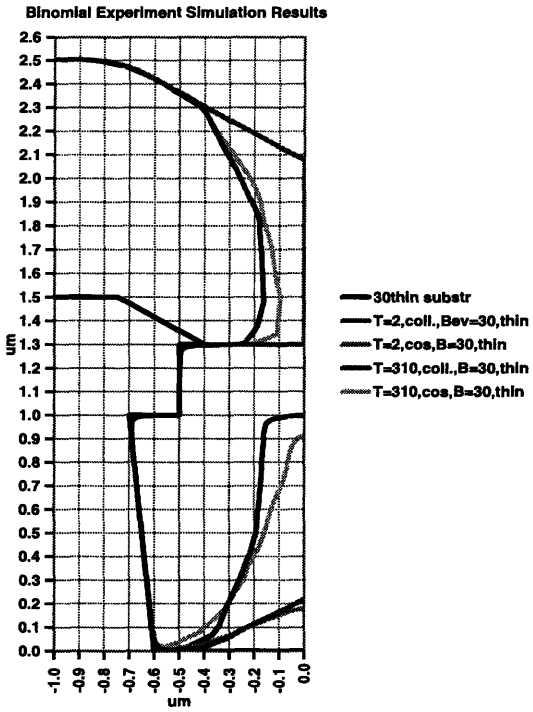

Figure 20: Deposition results on substrate with thin parting layer and 30 degree bevel.

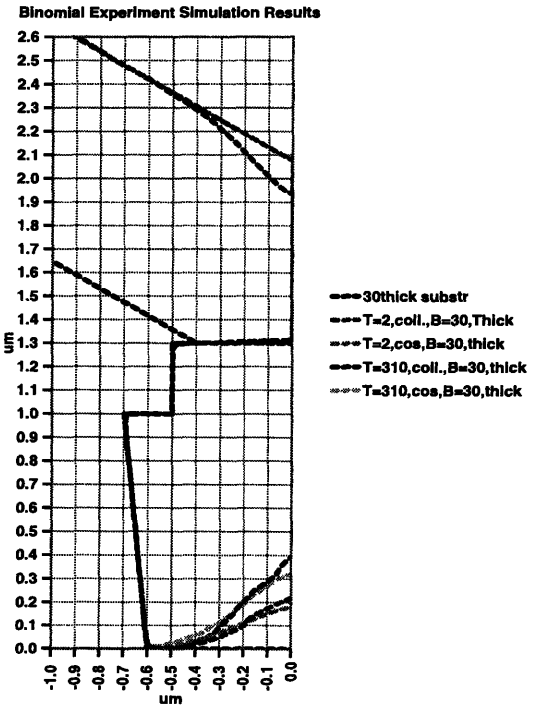

Figure 21: Deposition results on substrate with thick parting layer and 30 degree bevel.

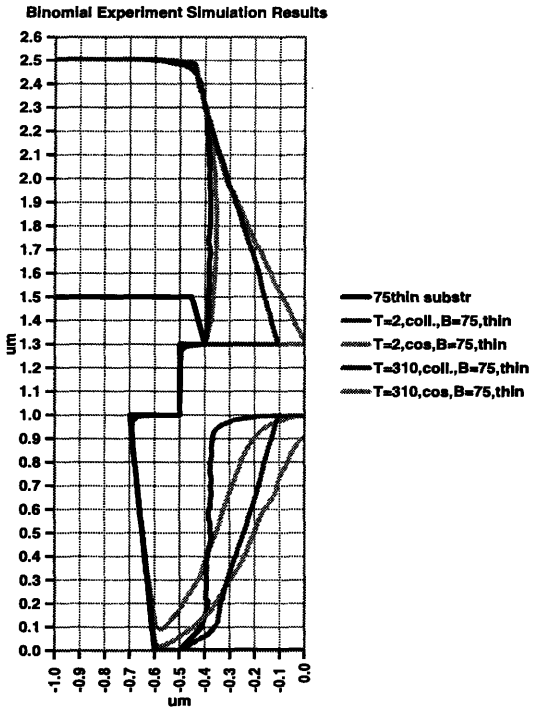

Figure 22: Deposition results on substrate with thin parting layer and 75 degree bevel.

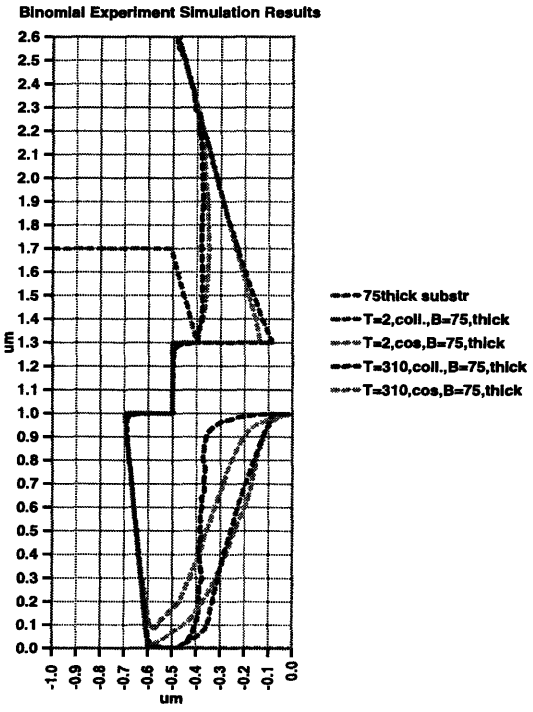

Figure 23: Deposition results on substrate with thick parting layer and 75 degree bevel.

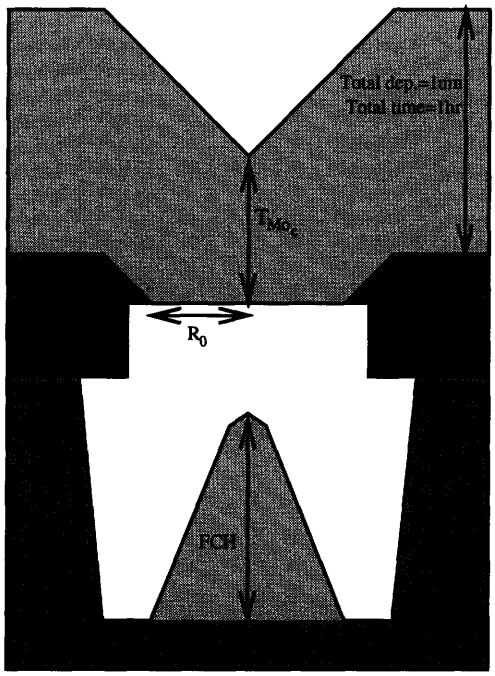

Figure 24: Graphical depiction of T_{Moc}, which is used to calculate the trench closure rate, TCR, of the simulation results.

flux rate was 1μm per hour, this thickness gave the amount of time that the trench was closed. The time it took for the trench to close is thus 1hr minus the time the trench was closed. By dividing the initial trench opening, .4μm, by this time, the TCR is found. In equation form, the trench closure rate is expressed as

$$TCR_{open\ trench} = \frac{(.4\mu m - Final\ Trench\ Radius)}{1hr} \tag{20}$$

$$TCR_{closed\ trench} = \frac{.4\mu m}{(1 - T_{Moc})hr} \tag{21}$$

For example, if at the end of a simulation T_{Moc} was .3μm, then that implies that the trench had been closed for $\frac{.3\mu m}{\frac{1\mu m}{hr}} = .3hr$. Thus, the trench was open for 1hr-.3hr=.7hr. The initial trench opening radius is .4μm, giving $TCR = \frac{.4\mu m}{.7hr} = .57\frac{\mu m}{hr}$.

The FCH was simply a measure of the height of the cone at the end of the deposition process (shown in Figure 24). This does not correspond directly to a growth rate, since cones will stop

growing as soon as the trench is closed. The CGR, on the other hand, was a measure of the rate at which the cone grew while the trench was open. For trenches which did not close, the CGR was equal to the FCH, since the total simulation time was one hour. For trenches which closed, however, the CGR was calculated by dividing the FCH by the time it took to close the trench. The cone growth rate, then, is

$$CGR_{open\ trench} = \frac{FCH}{1hr} \tag{22}$$

$$CGR_{closed\ trench} = \frac{FCH}{(1 - T_{Moc})hr}. \tag{23}$$

After these quantities were calculated for all 16 simulation results, the method described by Chung[13] was used to determine the relative importance of each of the four variables upon the three calculated quantities. For each simulation, each of the parameters was assigned a value of -1 or +1. The low temperature (2K), the perfectly collimated flux, the 30 degree parting layer bevel, and the .2μm parting layer thickness were assigned -1, and their counterparts were assigned +1. Thus, the sixteen simulations and their results were tabulated as in Table 1, found in appendix A.

Once this table was formed, the effect of each input parameter on the quantities TCR, FCH and CGR were calculated according to the following algorithm: To find the effect of parameter P on quantity Q, each value of Q_i was multiplied by the value of P_i (-1 or +1), where i represents an individual simulation. These results were summed together and divided by eight, effectively giving the average change in Q_i over all changes in P[13]. For example, the effect of changing temperature, T, upon the TCR was found by using the equation,

$$E_{T,TCR} = \frac{T_1TCR_1 + T_2TCR_2 + ... + T_{15}TCR15 + T_{16}TCR_{16}}{8}. \tag{24}$$

Note that the value of each T_i is either -1 or +1, not 2K or 310K.

In addition to single-parameter effects, the effects of interaction among all possible parameter pairs were calculated. To do this, the product $P_{A_i}P_{B_i}$ of the two parameters interacting, P_{A_i}

and P_{B_i} was multiplied by the quantity Q_i for all i. Just as for the single variable case, these terms were then summed and divided by eight[13]. Thus, the effect of the interaction between temperature and flux distribution, D, on the TCR was calculated according to

$$E_{TxD,TCR} = \frac{T_1 D_1 TCR_1 + T_2 D_2 TCR_2 + ... + T_{15} D_{15} TCR15 + T_{16} D_{16} TCR_{16}}{8}. \quad (25)$$

3.3.3 Results of Binomial Experiment Simulations

Table 2, found in appendix A, shows the calculated effects of each parameter and two-parameter interaction upon the TCR, FCH and CGR.

Since it is the relative importance of each parameter to each quantity that is sought, the magnitudes of the values in table 2 are normalized and listed in table 3, also found in appendix A. Note that the TCR and FCH columns are normalized with respect to the parting layer bevel effect, while the CGR column is normalized with respect to the flux distribution effect.

The parting layer bevel had the strongest effect upon both the TCR and the FCH. The effect was negative for TCR, implying that faster trench closure results with shallow parting layer bevelss. The effect was positive for the FCH, meaning that steeper bevels give taller cones. As one would expect, the effect of most parameters upon the TCR and upon the FCH were of opposite signs, since a faster closure rate gives less time for the cone to grow. The only exception to this was with the flux distribution/parting layer bevel interaction term, but this term had little effect on either quantity.

Also important to the TCR and FCH was the temperature. The TCR dependence upon temperature was negative, indicating that at high temperature, the trench closure occurs more slowly than at low temperatures. Temperature also positively affected the FCH, as well. The effect on these quantities due to temperature is primarly caused by surface diffusion occurring on the molybdenum layer on top of the parting layer, not on the actual emitter cone. At high temperature, the flux landing on the parting layer is able to diffuse, thus keeping the trench open, and allowing the cone to grow. Because the surface diffusion parameters cause surface diffusion to

be either "off" or "on," depending upon temperature, the measured effect of temperature upon the TCR, FCH, and CGR comes out to be quite large. Of course temperature is very important to these quantities, but in reality, a process will most likely be strongly in one regime of operation, so no variation will be noticed. For the molybdenum surface diffusion data obtained in the literature, the cone deposition process would definitely take place in the regime of operation where surface diffusion is negligible.

The thickness affected the three quantities measured, but it was not a dominant parameter. Increasing the thickness acted to increase the TCR, decrease the FCH, and increase the CGR. This result contradicted the decrease in the trench closure rate observed in the preliminary experiments.

The CGR quantity revealed some very interesting behavior of the cone deposition process. Unlike the TCR and FCH quantities, which were dominated by the parting layer bevel, the CGR was controlled primarily by the flux distribution. It varied negatively with flux distribution, meaning that the CGR decreased with wider flux distributions. The interaction term of flux distribution and parting layer bevel also had a strong effect upon the CGR. This was particularly interesting, since this interaction term was also the only term which contributed positively to both the TCR and the FCH. Furthermore, of the four parameters investigated, temperature and parting layer thickness are parameters which can be easily controlled in a processing environment, while parting layer bevel and flux distribution are more difficult to monitor and control.

3.4 Parting Layer Bevel and Flux Distribution Simulations

3.4.1 Parameter Variations Used

With this in mind, another set of simulations was conducted, in which temperature was fixed at 2K, the thin ($.2\mu$m) parting layer was used, and the flux distribution and parting layer bevel were varied. The same two flux distributions were used in this set of simulations as in the binomial set, but in this set, nine different bevel values were used, ranging from 50 degrees to 90 degrees in increments of 5 degrees. This set of simulations was run in order to examine the effects of process

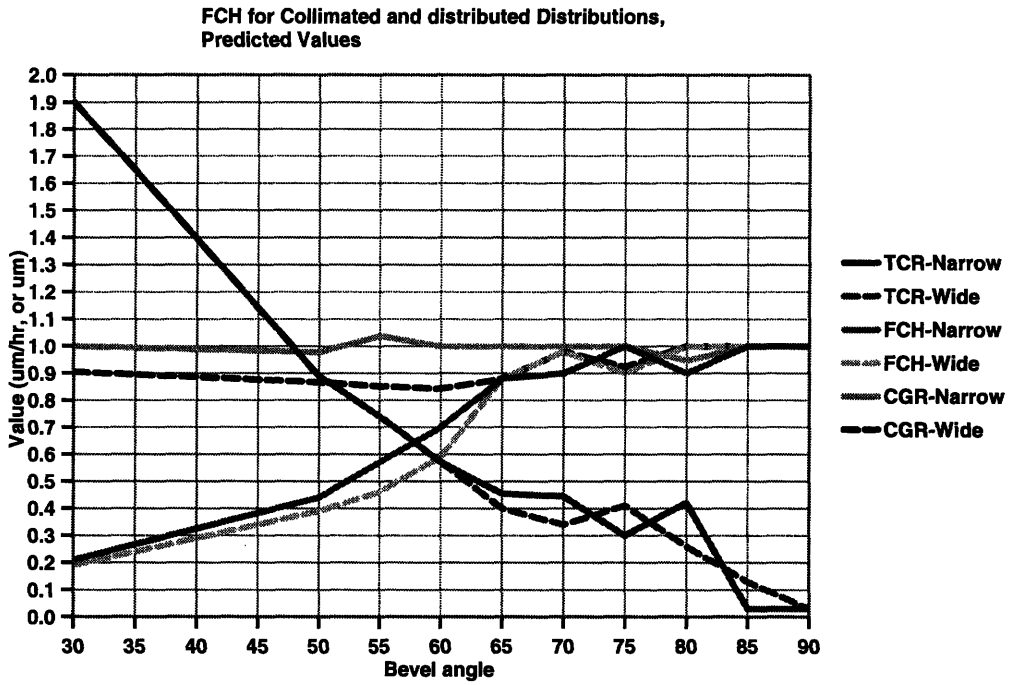

Figure 25: TCR, FCH, and CGR data for Parting Layer Bevel/Flux Distribution simulations.

variation and possible nonuniformities across a substrate on which cones are deposited.

3.4.2 Results

The results of this set of simulations revealed some definite trends in the TCR, FCH, and CGR. Figure 25 plots the TCR, FCH, and CGR for both the collimated and $\cos^{100}(\theta)$ flux distributions. The datapoints for parting layer bevels of 30 and 75 degrees were taken from the previous set of experiments.

The CGR curves are clearly different for the collimated and $\cos^{100}(\theta)$ flux distributions. For bevels below 80 degrees, the CGR of the $\cos^{100}(\theta)$ flux distribution is consistently about 10% less than that of the collimated distribution. For very sharp parting layer bevels, the two curves merge. This is probably due to the fact that for higher bevels, the trench never closes, and the cones grow to their full height. The CGR for simulations using the collimated flux is always very close to the flux rate, 1μm per hour. This is the result which was expected, since a perfectly collimated flux will build up the cone for the entire time the trench is open. A distributed flux will also build the cone whenever the trench is open, but since the *total* rate of flux integrated over

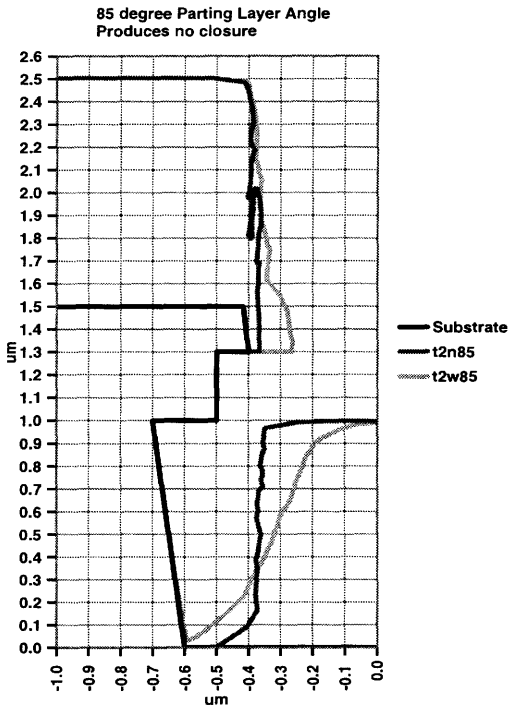

Figure 26: Results showing no trench closure occurring for 85 degree parting layer bevel.

all angles is 1μm per hour, the flux arriving at vertical incidence will be less than this. Therefore, for trenches where only very vertically-directed flux can arrive, a distributed flux will produce a smaller CGR than a collimated flux.

The FCH curve showed that the final height of the deposited cones increases with increasing parting layer bevel and eventually reaches 1μm for parting layer bevels above 80 degrees. Note, however, that at these bevels, no trench closure occurs, so a vertical "pillar" is formed instead of a cone. This is plotted in Figure 26. For parting layer bevels 65 degrees and less, the collimated distribution gave a higher FCH for cones deposited on the same substrate. For higher bevels, however, this pattern disappeared. The FCH of one flux distribution was not consistently larger than the other.

The TCR curve in Figure 25 and the graphs of the resulting cone profiles yielded the most interesting results of this set of simulations. Examination of the resulting molybdenum profiles on top of the trench revealed that nearly all the profiles intersected at a point 1μm above the edge

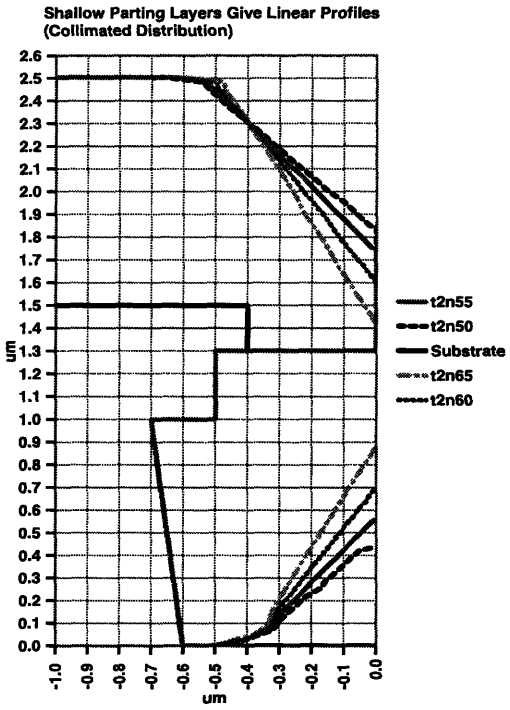

Figure 27: Deposition of collimated flux for parting layer bevels below 70 degrees gives common intersection point and a linear profile.

of the parting layer overhanging the trench.

It was also observed that for simulations using the collimated distribution and parting layer bevels up to 70 degrees, the profiles were linear, and they maintained the same angle relative to horizontal as the substrates onto which they were deposited. These profiles are plotted in Figure 27. For parting layer bevels 70 degrees and greater, the profiles still intersected at the same point, but they did not maintain the linear shape. These are shown in Figure 28. For the simulations using the $\cos^{100}(\theta)$ distribution, the profiles obeyed the linear behavior only with parting layer bevels less than 60 degrees. These results are plotted in Figures 29 and 30.

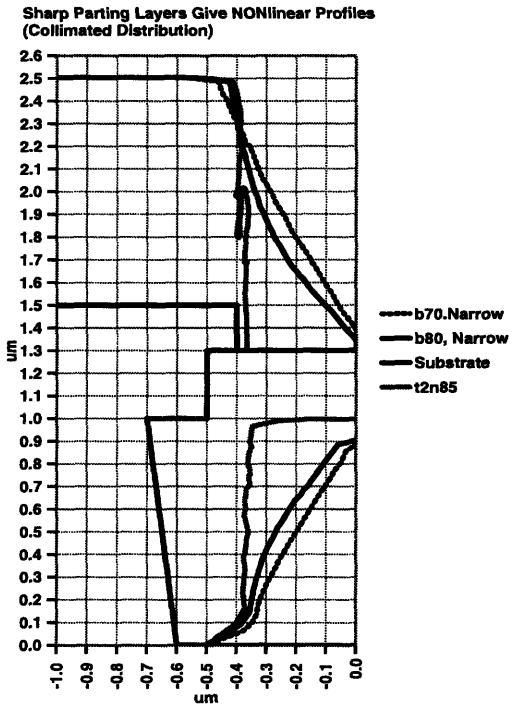

Figure 28: Deposition of collimated flux for parting layer bevels 70 degrees and above gives non-linear profile.

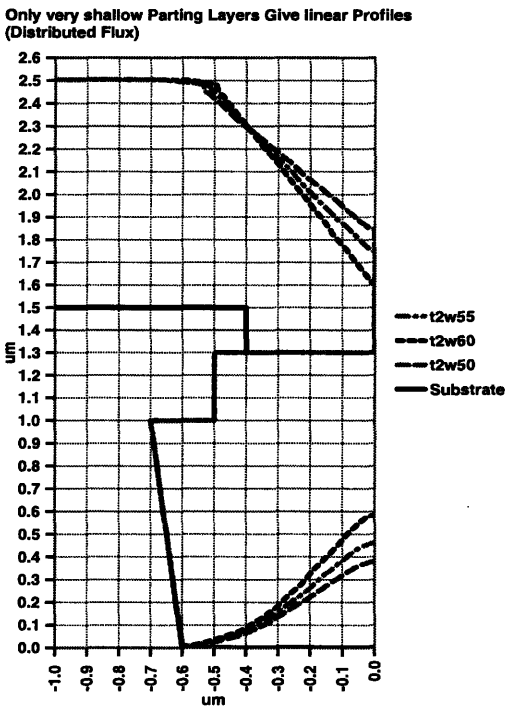

Figure 29: Deposition of $\cos^{100}(\theta)$ flux for parting layer bevels below 65 degrees results in linear profile.

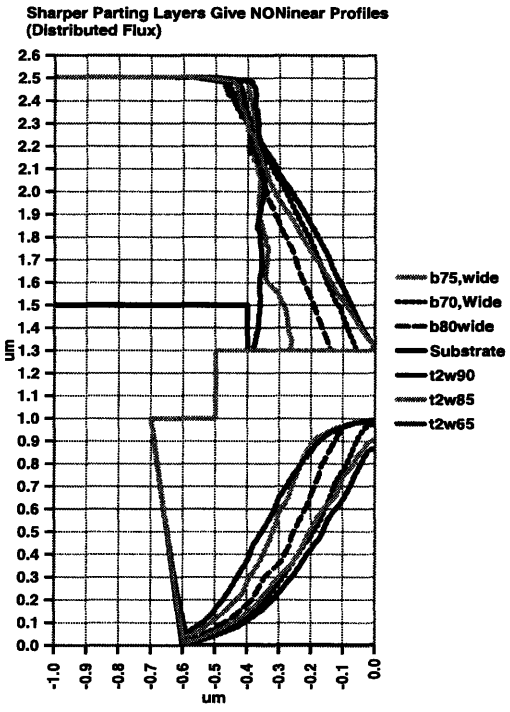

Figure 30: Deposition of $\cos^{100}(\theta)$ flux for parting layer bevels above 60 degrees gives very non-linear profile.

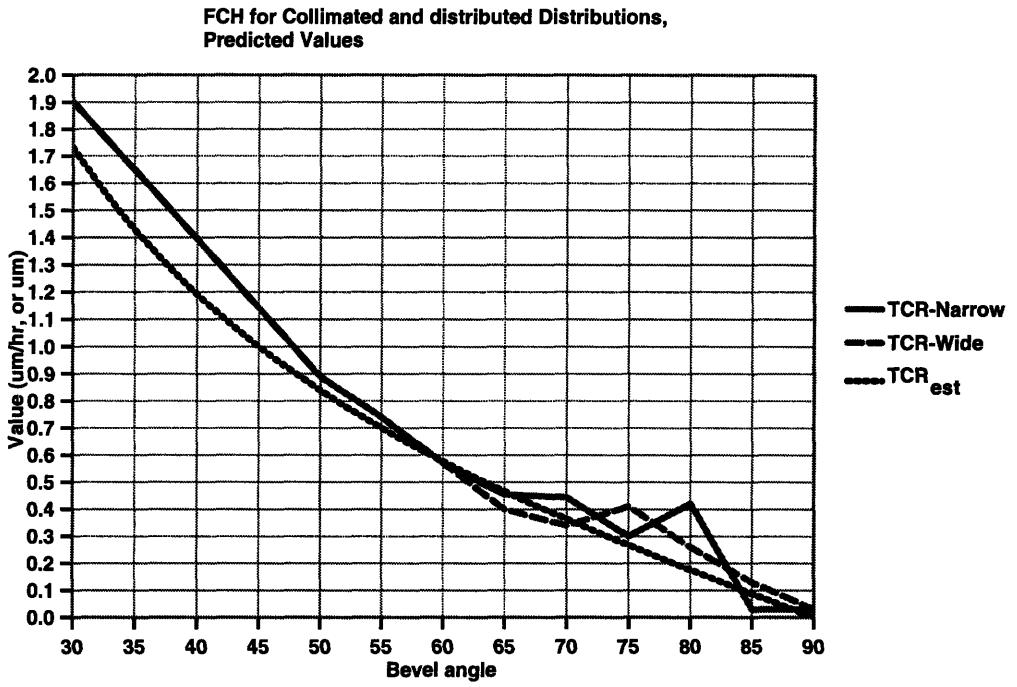

Figure 31: Measured TCR's for narrow and wide flux distributions and $TCR_{est.}$

3.4.3 Predicting the Cone Shape

Using these observations and elementary trigonometry, the trench closure rate for those profiles having the linear profile can be estimated as

$$TCR_{est.} = \frac{\Phi}{tan(\psi)}, \tag{26}$$

where Φ is the rate of flux and ψ is the parting layer bevel. Figure 31 plots the calculated TCR's for the simulations as well as $TCR_{est.}$. The agreement between the measured TCR's of simulations using the collimated flux distribution and $TCR_{est.}$ is quite good for parting layer bevels less than 70 degrees. For a distributed flux, this agreement holds only with parting layer bevels less than 60 degrees.

The result above indicates that if the parting layer bevel of a substrate is known and is sufficiently shallow (depending upon the flux distribution), the TCR can be predicted by Equation 26.

An expression for the FCH can be written in terms of the CGR, the TCR, and the initial

trench opening radius, R_0,

$$FCH = CGR\frac{R_0}{TCR}. \tag{27}$$

Note that $\frac{R_0}{TCR}$ is the amount of time the trench will be open, and is thus the amount of time that the cone will grow.

From the simulation results, it appears sufficient to model the CGR as a fraction, p, of the rate of flux, Φ. For a collimated flux distribution, $p = 1$. The CGR data in Figure 25 indicates that for the $\cos^{100}(\theta)$ distribution, $p = 0.9$.

Thus, Equation 26 and the expression for the CGR may be substituted into Equation 27 to give

$$FCH_{est.} = p\Phi\frac{R_0}{\frac{\Phi}{tan(\psi)}} = pR_0tan(\psi) \tag{28}$$

Figure 32 lists the calculated and predicted values of FCH for all the simulations run. The agreement between actual and predicted values for the collimated distribution is excellent for parting layer bevels up to 70 degrees. The agreement is not as good for simulations using the $\cos^{100}(\theta)$ distribution.

Just as $FCH_{est.}$ can be calculated as a function of R_0 and ψ, so can ψ be calculated for a given FCH and R_0. This allows for the calculation of the parting layer bevel needed to produce a cone with a given radial aspect ratio, $\frac{FCH}{R_0}$.

An ideal cone is formed when the cone comes to a point at the top of the trench. Rearranging Equation 28, and replacing FCH with D, the depth of the trench, gives

$$tan(\psi) = \frac{1}{p}\frac{D}{R_0}. \tag{29}$$

Solving for ψ gives the expression

$$\psi = tan^{-1}(\frac{A}{p}), \tag{30}$$

where $A = \frac{D}{R_0}$, the radial aspect ratio of the trench. This equation states the requirement on ψ when fabricating cones with an aspect ratio of $\frac{D}{R_0}$.

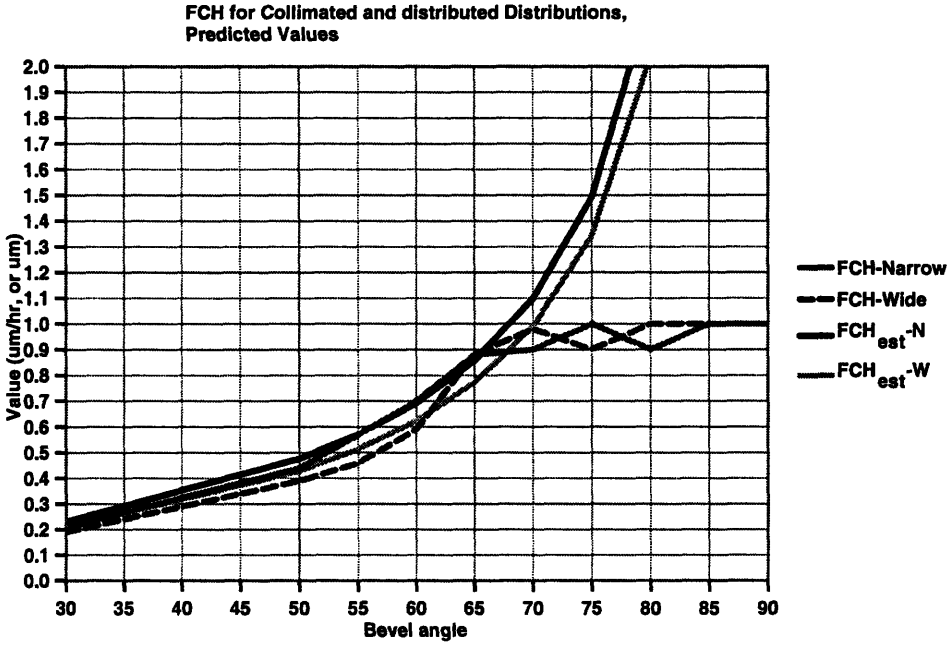

Figure 32: Measured and Estimated values of FCH for both collimated and $\cos^{100}(\theta)$ flux distributions.

The substrate used in these simulations had a depth, $D = 1\mu$m, and an initial opening radius, R_0=.4μm, giving an aspect ratio of 2.5. Thus, to find the parting layer bevel that will yield an ideal cone, these values are subtituted into equation 30, giving,

$$\psi_{coll.} = tan^{-1}(\frac{2.5}{1}) = 68.20\ degrees \tag{31}$$

for a collimated flux and

$$\psi_{cos^{100}(\theta)} = tan^{-1}(\frac{2.5}{0.9}) = 70.20\ degrees \tag{32}$$

for the distributed flux. Note that $\psi_{cos^{100}(\theta)}$ is greater than 60 degrees, the maximum bevel for which the cone heights could be predicted for the $\cos^{100}(\theta)$ flux. On the other hand, $\psi_{coll.}$ is still in the range where the model is accurate. Figures 33 and 34 show substrates with parting layer bevels of 68.2 degrees and 70 degrees, repectively. The cone in Figure 33 is nearly perfect; it it 1μm tall, and the trench is less than .03μm away from closure. Figure 34 shows that the

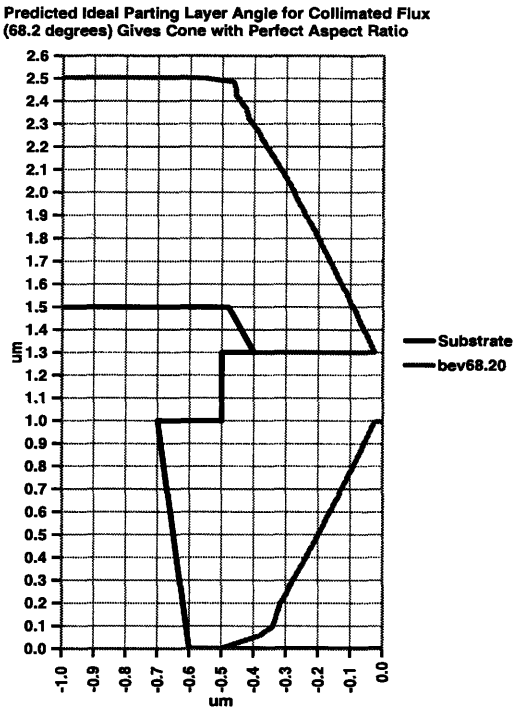

Figure 33: Cone deposited onto substrate with ideal estimated parting layer bevel for collimated distribution. Resulting cone has ideal aspect ratio.

prediction was fairly accurate for the $\cos^{100}(\theta)$ distributed flux, as well. This may be a fluke, however, because the resulting cone height produced with ψ=65 degrees does not agree with the predicted value (see Figure 32.) This is an indication that a more widely distributed flux makes prediction of the FCH less reliable. Another item to notice is that the base width of the cone deposited with the $\cos^{100}(\theta)$ flux is much wider than the cone produced using the collimated flux.

It is desirable to produce cones with high aspect ratios. The predicted necessary value of $\psi_{coll.}$ and $\psi_{cos^{100}(\theta)}$ to produce such cones increases for higher aspect ratios. Unfortunately, these predicted values quickly fall out of the range of the model's accuracy. This implies that it is more difficult to predictably produce cones with higher aspect ratios. Figure 35 shows a plot of $\psi_{coll.}$ and $\psi_{cos^{100}(\theta)}$ as a function of the desired trench aspect ratio.

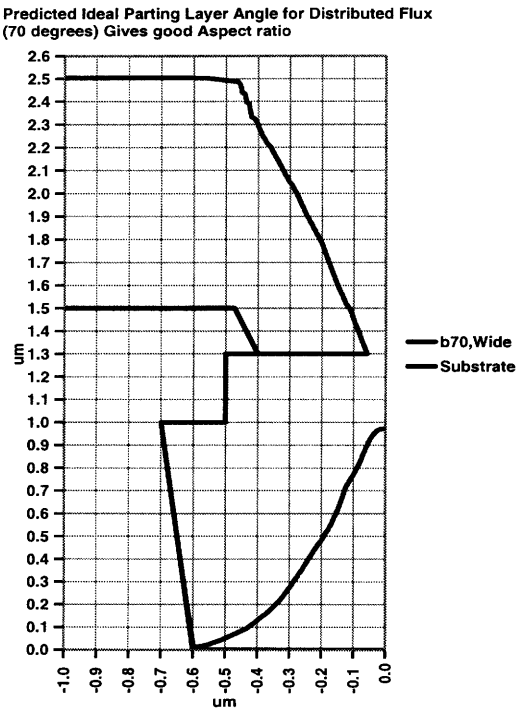

Figure 34: Cone deposited onto substrate with ideal estimated parting layer bevel for $\cos^{100}(\theta)$ distribution. Resulting cone has aspect ratio close to ideal.

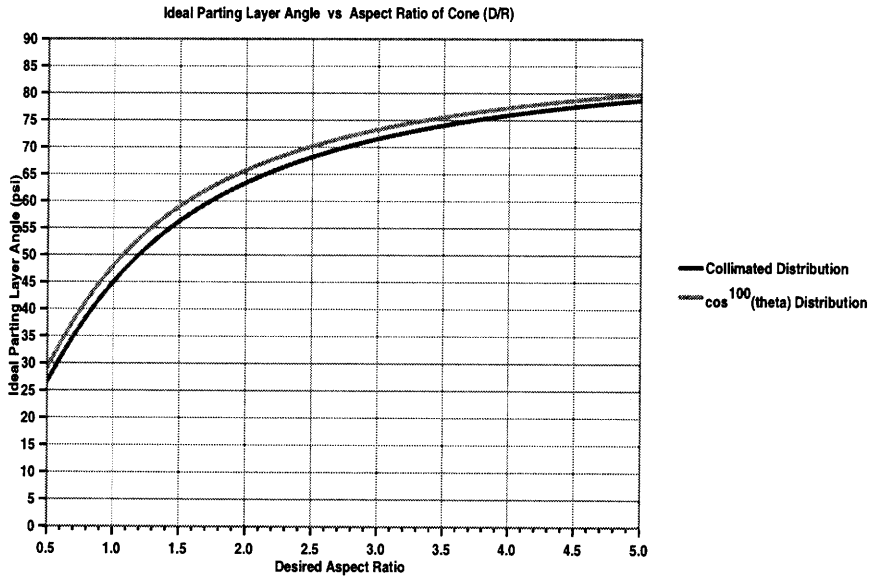

Figure 35: $\psi_{coll.}$ and $\psi_{cos^{100}(\theta)}$ versus desired trench aspect ratio.

4 Future Work

There exists a multitude of additional avenues of investigation which can be followed to further the results of this study. Although much has been learned about the relative effects of the four parameters studied— temperature, parting layer bevel, parting layer thickness, and flux distribution— the quantification of these effects was not achieved. Additional simulations or actual laboratory experiments may provide the information needed to allow a truly quantitative description of the effect of each parameter upon the cone geometry.

Surface diffusion experiments at temperatures near room temperature should be performed. All diffusion data presently available for molybdenum is based on experiments conducted at temperatures greater than 50% of its melting temperature. Room temperature experiments may show that the diffusion coefficient for molybdenum is not actually as low as current data indicates. If so, then surface diffusion may be an important parameter at the temperatures used in cone deposition processes.

Further work can be done using a numerical simulation program like that written by the author. A refinement of the numerical methods for calculating the profile derivatives will remove the instability problems experienced. This will allow the use of physically realistic paramaters and will thereby produce more meaningful results. The discovered importance of the parting layer upon the deposition process warrants that the geometry of this layer be included in future programs. This would simulate the process more realistically, and incorporate the effects of geometry-dependent trench closure rates.

Depositing cones comprised of two materials may be useful for placing resistive layers at the base of each emitter. Simulations of these two-material depositions may help to ascertain the feasability of this. Figures 36-38 show example 2-material distributions. Figure 36 shows the result of a deposition of a material with a low diffusion coefficient followed by the deposition of a material with a high diffusion coefficient. Figure 37 shows the result of the running the depositions in reverse order, and Figure 38 shows the result of depositing 2 materials each with low diffusion

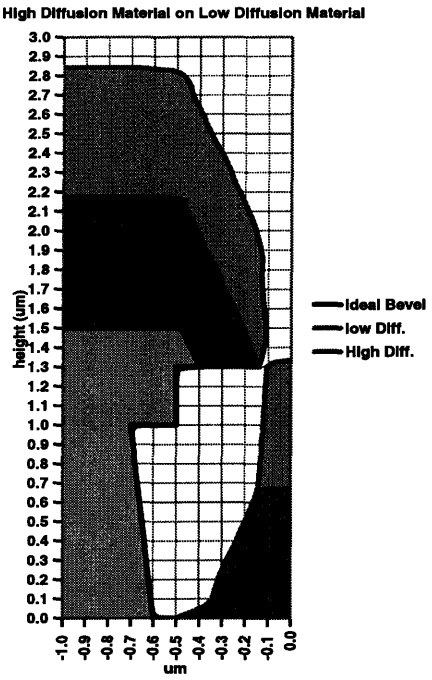

Figure 36: 2-material deposition. Highly diffusive material deposited onto nondiffusive material.

coefficients. These simulations are in agreement with the observations made in the single-material simulations. Namely, a sharp point at the inner edge of the topmost layer is needed in order for trench closure to occur. Notice in Figures 36 and 37 that the deposition of a highly diffusive material eliminates that edge, preventing any further trench closure.

The thickness of the parting layer was shown to have a small effect upon the trench closure rate and the final cone height in the binomial experiment set of simulations. The nature of this effect is not understood, and it could be very important to the scaling of the devices. Simulation sets in which several parting layer thicknesses are used may provide answers as to how the thickness affects the cone evolution.

At high parting layer bevels, the trench closure becomes more complicated. The rate of trench closure does not monotonically decrease, as it does for parting layer bevels less than 70 degrees. The model for predicting the FCH, which is very accurate for bevels less than 70 degrees, becomes quite inaccurate above this value. Clearly there is some mechanism causing this behavior which

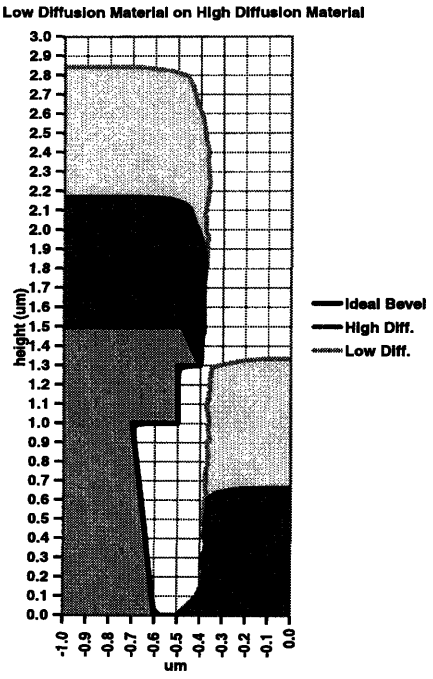

Figure 37: 2-material deposition. Nondiffusive material deposited onto highly diffusive material.

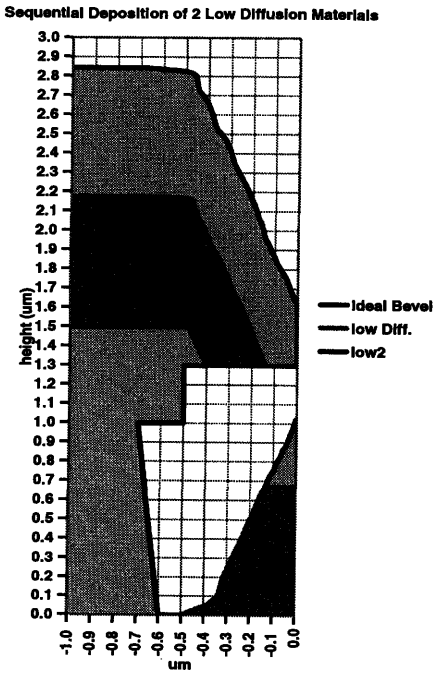

Figure 38: 2-material deposition. Two nondiffusive materials deposited in series.

should be studied. By examining the difference between the predicted and achieved cone height as a function of parting layer bevel, this mechanism may be better understood.

Simulations of cone depositions using flux distributions intermediate to perfect collimation and $\cos^{100}(\theta)$ may reveal more clearly the role of flux distribution in the process. The effect of the flux distribution on p, the fraction of the flux which determines CGR, is another important quantity. The relationship between the flux distribution and the CGR is probably not the simple linear one used in predicting the cone heights.

The interaction between parting layer bevel and flux distribution should also be examined in more depth, since these two parameters are not as easily controlled as process temperature or parting layer thickness. Parting layer bevels may vary for emitters across a substrate due to variations in etch directionality. The degree of flux collimation depends upon the deposition equipment being used.

5 Conclusions

Field emitter arrays (FEA's) are a potentially excellent technology for flat panel display applications. They make use of the performance advantages of the cathode ray tube, while maintaining the small size of the liquid crystal display. The shape of the emitter cone is important to to the performance of FED's. A small radius of curvature at the tip of the cone is desirable for high emission efficiency. A tall cone is beneficial, in that it decreases the gate to emitter capacitance. This increases the switching speed of the device and decreases dynamic power dissipation. This study has investigated how temperature, parting layer bevel, parting layer thickness, and flux distribution affect the resulting shape of deposited emitter cones.

The affect of temperature is that it activates surface diffusion. The presently available data for molybdenum indicates that at the temperatures used in the fabrication of FED's, surface diffusion is negligible. The published surface diffusion values for aluminum give an extremely sharp turn-on of surface diffusion near room temperature. Over a very small temperature range, surface diffusion increases from being essentially zero to being highly activated. This led to the conclusion that the deposition process will take place when one of these two regimes is applicable. Thus, although temperature is an important parameter, it does not require precise control.

It was shown that in the fabrication of FED's, materials with low diffusion coefficients should be sought for the emitters. A numerical computer simulation demonstrated that cones formed using materials with high surface diffusion coefficients will spread out during high temperature steps. The tip radius of curvature increases with these annealling steps, and thereby degrades the current emission efficiency of the devices.

A high surface diffusion coefficient also causes the flux landing on the parting layer to redistribute and grow vertically. This prevents the trench from closing, thereby preventing the fabrication of useful cones. It was this effect— surface diffusion of the molybdenum on top of the parting layer— not the surface diffusion of the actual cone, which was important to the evolution of the cones.

In order for the trench to close at all, a specific substrate is required. The parting layer must exhibit a bevelled sidewall, and it must come to a sharp point at the opening of the trench. This may impose restrictions on how the gate layer is etched and how the parting layer is deposited.

The thickness of the parting layer influenced the cone evolution, although its importance was small compared to that of temperature and parting layer bevel. The different simulation sets produced contradictory results, showing both smaller and larger trench closure rates for larger parting layer thicknesses. Thus, the effect of parting layer thickness upon done evolution was not determined.

The parting layer bevel was the most important parameter to the cone deposition process. Trenches with shallow (low) parting layer bevels closed very rapidly, while trenches with sharp (high) bevels did not close at all.

The degree of flux collimation was important in determining the resulting cone shape. A wide flux distribution resulted in cones with wider bases and slower growth rates than the collimated distribution. The cone growth rate was also affected by the interaction of the flux distribution with the parting layer bevel. Unlike temperature and parting layer thickness, the parting layer bevel and the flux distribution are not easily controlled or monitored. Because these parameters may be nonuniform across a wafer, a set of simulations was conducted to determine the effect of varying them on the cone evolution.

In this set, temperature was fixed low, since that more accurately depicts the surface diffusion coefficient of molybdenum. The parting layer thickness, was fixed at $.2\mu$m.

The results showed that the shallow parting layer bevels yield a predictable cone height, up to parting layer bevels of 70 degrees for collimated distributions, and 60 degrees for the $\cos^{100}(\theta)$ distribution that was used.

For substrates with parting layer bevels less than these, the trench closure rate was estimated as

$$TCR_{est.} = \frac{\Phi}{tan(\psi)}, \tag{33}$$

where Φ is the rate of flux and ψ is the parting layer bevel. The predicted final cone height was

$$FCH_{est.} = pR_0 tan(\psi), \tag{34}$$

where R_0 is the initial trench opening radius and p is a function of the flux distribution. These equations are in good agreement with the simulation results for low parting layer bevels.

For sharper parting layers, the trench closure rate becomes unpredictable. The distributed flux was shown to make the resulting cone height less predictable, particularly at higher parting layer bevels. These are warnings that it may be difficult to optimize a process for producing cones with high aspect ratios, since such cones require high parting layer bevels, and since flux distribution cannot be perfectly controlled.

This study has identified the important parameters affecting the field emitter cone deposition process. It is hoped that this new information will aid future research efforts to understand the process more quantitatively.

6 Appendix A: Tables of Results from Binomial Set of Simulations

The following tables are included in this section:

1. Table 1. The matrix of all 16 experiments. Each parameter value is assigned a value of -1 or +1. The TCR, FCH, and CGR measured for each simulation are listed.
2. Table 2. This lists the calculated effect of each parameter and parameter pair on the TCR, FCH, and CGR.
3. Table 3. This is a normalized version of table 2. The TCR and the FCH are normalized by the effect of the parting layer bevel, and the CGR is normalized by the effect of the flux distribution.

In each table, the following abbreviations are used:

1. T= Temperature variable value. -1 refers to 2K, and +1 refers to 310K.
2. B= Parting Layer Bevel. -1 refers to 30 degree bevel, and +1 refers to 75 degree bevel.
3. D= Distibution of flux. -1 refers to the collimated flux, and +1 refers to the $\cos^{100}(\theta)$ distributed flux.
4. K= Parting layer thickness. -1 refers to the .2μm thick parting layer, and +1 refers to the .4μm thick parting layer.
5. Interaction terms are represented by $X * Y$, where X and Y are the two parameters interacting.
6. TCR= Trench closure Rate (see section 3.3.2).
7. FCH= Final cone height (see section 3.3.2).
8. CGR= Cone growth rate (see section 3.3.2).

	TABLE 1: EXPERIMENTAL MATRIX															
	T	D	B	K	T*D	T*B	T*K	D*B	D*K	B*K	TCR (um/hr)		FCH (um)		CGR (um/hr)	
	-1	-1	-1	-1	1	1	1	1	1	1	1.9		0.21		1	
	-1	-1	-1	1	1	1	-1	1	-1	-1	1.9		0.21		1	
	-1	-1	1	-1	1	-1	1	-1	1	-1	0.3		1		1	
	-1	-1	1	1	1	-1	-1	-1	-1	1	0.31		1		1	
	-1	1	-1	-1	-1	1	1	-1	-1	1	1.9		0.19		0.905	
	-1	1	-1	1	-1	1	-1	-1	1	-1	1.9		0.19		0.905	
	-1	1	1	-1	-1	-1	1	1	-1	-1	0.4		0.9		0.9	
	-1	1	1	1	-1	-1	-1	1	1	1	0.26		1		1	
	1	-1	-1	-1	-1	-1	-1	1	1	1	0.24		1		1	
	1	-1	-1	1	-1	-1	1	1	-1	-1	1.11		0.4		1.11	
	1	-1	1	-1	-1	1	-1	-1	1	-1	0.02		1		1	
	1	-1	1	1	-1	1	1	-1	-1	1	0.02		1		1	
	1	1	-1	-1	1	-1	-1	-1	-1	1	0.3		0.9		0.9	
	1	1	-1	1	1	-1	1	-1	1	-1	1.11		0.31		0.861	
	1	1	1	-1	1	1	-1	1	-1	-1	0.05		1		1	
	1	1	1	1	1	1	1	1	1	1	0.05		1		1	

TABLE 2: Calculated Effects of Each Parameter			
Effects:	TCR	FCH	CGR
T	-0.748	0.239	0.0203
D	0.0213	-0.0413	-0.0801
B	-1.12	0.561	0.0273
K	0.194	-0.136	0.0215
T*D	0.00875	-0.00625	-0.00744
T*B	0.466	-0.214	0.00466
T*K	0.227	-0.161	-0.00347
D*B	0.00625	0.0162	0.0551
D*K	-0.0263	0.0138	-0.00625
B*K	-0.227	0.161	0.00347

TABLE 3: Normalized Effects of Each Parameter			
Effects:	TCR	FCH	CGR
T	-0.667	0.425	0.254
D	0.0189	-0.0735	-1
B	-1	1	0.341
K	0.173	-0.243	0.269
T*D	0.0078	-0.0111	-0.0929
T*B	0.415	-0.381	0.0582
T*K	0.202	-0.287	-0.0434
D*B	0.00557	0.029	0.688
D*K	-0.0234	0.0245	-0.0781
B*K	-0.202	0.287	0.0434

7 Acknowledgements

The author would like to give special thanks to David Bang for his helpfulness with SPEEDIE, Thomas Sunn Pedersen for his advice on the numerical program, Peining Wang for her programming lessons, and to Jill and Haleigh, who were always around to keep me motivated.

8 References

[1]Gray, Henry. "The Field-Emitter Display." Information Display, March 1993.

[2]Spindt, C. A., I. Brodie, L. Humphrey, and E. R. Westerberg, IEEE Transactions on Electron Devices, Vol 36, No. 1, January 1989.

[3]Bozler, Carl O., Harris, Christopher T., Rabe, Steven, Rathman, Dennis D., Hollis, Mark A., Journal of Vacuum Science and Technology B., Vol 12, No. 2, March/April 1994.

[4]Spindt, C. A., I. Brodie, L. Humphrey, and E. R. Westerberg, Journal of Applied Physics, Vol. 47, No. 12, Dec. 1976.

[6]Utsumi, Takao. "Vacuum Microelectronics: What's New and Exciting." Keynote Address, IEEE Transactions on Electron Devices, Vol 38, No. 10, October 1991.

[7]Akinwande, Ibitayo. Personal communication.

[8]Neumann, Gerhard. "Surface self-diffusion of metals." Bay Village, Ohio: Diffusion Information Center, 1972.

[9]Mullins, W. W., Journal of Applied Physics, Vol. 28, No.3, March. 1957.

[10]Cale, T.S., Jain, Monoj K., Taylor, Donald S., Journal of Vacuum Science and Technology B., Vol 11, No. 2, March/April 1993.

[11]Wohlbier, F.H., ed. "Metals and Alloys." Diffusion and Defect Data, Vol 21, 1980.

[12]W. R. Tyson, W. A. Miller, Surface Science, Vol. 62, 1977.

[13]Chung, Ho. "Concept of Experiment Design for Product and Process Optimization." Honeywell, Inc.

[14]A. Ghis, R. Meyer, P. Rambaud, F. Levy, and T. Leroux, IEEE Transactions on Electron Devices, Vol 38, No. 10, 1991.

[15]P. Vaudaine, R. Meyer., IEDM 91.

[16]C. L. Liu et al., Surface Science, Vol 253, 1991.

[17]Pankove, J. I., ed. "Display Devices." Topics in Applied Physics, Vol 40, 1980.

[18]Wohlbier, F.H., Fisher, D.J., ed. Diffusion and Defect Data, Vol 27, 1982.